Zwitterionic Brush-Grafted Interfacial Bio-Lubricant Evades Complement C3-Mediated Macrophage Phagocytosis for Osteoarthritis Therapy

Advanced Materials

Cai, Chuandong; Wang, Mingwei; Wang, Luman; Guo, Jiangtao; Wang, Lipeng et al

https://doi.org/10.1002/adma.202501137

ADVANCED MATERIALS
www.advmat.de

Zwitterionic Brush-Grafted Interfacial Bio-Lubricant Evades Complement C3-Mediated Macrophage Phagocytosis for Osteoarthritis Therapy

Chuandong Cai, Mingwei Wang, Luman Wang, Jiangtao Guo, Lipeng Wang, Yingkai Zhang, Guohao Wu, Bingxuan Hua, Martien A. Cohen Stuart,* Xuhong Guo,* Lu Cao,* and Zuoqin Yan**

Administering a bio-lubricant is a promising therapeutic approach for the treatment of osteoarthritis (OA), in particular, if it can both manage symptoms and halt disease progression. However, the clearance of these bio-lubricants mediated by synovial macrophages leads to reduced therapeutic efficiency and adverse inflammatory responses. Herein, it is shown that this process is predominantly mediated by the specific binding of complement C3 (on nanoparticle) and CD11b (on macrophage). More importantly, through a systematic evaluation of various interface modifications, a macrophage-evading nanoparticle strategy is proposed, which not only minimizes friction, but also largely suppresses C3 adsorption. It involves employing a zwitterionic poly-2-methacryloyloxyethyl phosphorylcholine (PMPC) brush layer grafted from a crosslinked gelatin core. In vitro studies demonstrate that such a nanoparticle lubricant can evade macrophage phagocytosis and further prevent the pro-inflammatory M1 polarization and subsequent harmful release of cytokines. In vivo studies show that the designed PMPC brush layer effectively mitigates synovial inflammation, alleviates OA-associated pain, and protects cartilage from degeneration, thus preventing OA progression. These findings clarify the pivotal role of complement C3-mediated macrophage recognition in nanoparticles clearance and offer a promising nanoparticle design strategy to restore joint lubrication.

1. Introduction

Osteoarthritis (OA) is a prevalent chronic "wear-tear" disease marked by the degeneration of articular cartilage, affecting over 500 million people worldwide and incurring substantial social and economic costs.[1] Owing to the non-regenerative properties of articular cartilage, the deterioration of OA is currently considered irreversible.[2] With the progression of OA, the damage of articular cartilage will be further aggravated, eventually leading to joint dysfunction or disability.[3] At present, clinical strategies for OA are limited to attenuating inflammation and relieving pain, which cannot effectively prevent the progression of the disease radically.[4]

Nanomedicines have promising potential for the treatment of OA.[5] Lubrication dysfunction is the primary factor of OA progression, leading to the continuous wear of articular cartilage.[6] Injecting nano-sized bio-lubricants into the joint cavity can effectively maintain the low

C. Cai, L. Wang, L. Wang, Y. Zhang, G. Wu, B. Hua, L. Cao, Z. Yan
Department of Orthopaedic Surgery
Zhongshan Hospital
Institute of Bone and Joint Diseases
Fudan University
Shanghai 200032, China
E-mail: cao.lu@zs-hospital.sh.cn; yan.zuoqin@zs-hospital.sh.cn

Z. Yan
Department of Orthopaedic Surgery
Shanghai Geriatric Medical Center
2560 Chunshen Road, Shanghai 201104, China

M. Wang, J. Guo, M. A. C. Stuart, X. Guo
School of Chemical Engineering
State-Key Laboratory of Chemical Engineering and Shanghai Key Laboratory of Multiphase Materials Chemical Engineering
East China University of Science and Technology
Shanghai 200237, China
E-mail: mingweiwang@ecust.edu.cn; martien.cohenstuart@gmail.com; guoxuhong@ecust.edu.cn

M. Wang
Department of Dentistry-Regenerative Biomaterials
Radboud University Medical Center
Nijmegen 6525 EX, The Netherlands

M. A. C. Stuart
Physical Chemistry and Soft Matter
Wageningen University and Research
Wageningen 6708 WE, The Netherlands

The ORCID identification number(s) for the author(s) of this article can be found under https://doi.org/10.1002/adma.202501137

DOI: 10.1002/adma.202501137

friction property and disperse the mechanical stress across the cartilage surface,[7] thereby preventing the wear and tear of the cartilage and halting the progression of OA at its early stage. However, injected nanomedicines must first survive the attack of the innate immunity system and then exert their therapeutic effects.[8] Synovial macrophages, the key mediator of innate immunity within the joint,[9] play a pivotal role in this process by recognizing and phagocytosing nanoparticles (NPs). This not only reduces the local concentration of NPs, necessitating more frequent injections, but also triggers the release of harmful cytokines from activated synovial macrophages, further exacerbating joint inflammation. These events therefore create a vicious cycle: loss of lubricant, exacerbation of joint inflammation, and repeated injections. Therefore, to identify and inhibit the signals that trigger synovial phagocytosis is highly desired to break the vicious cycle.

During systemic administration, the process of macrophage phagocytosis of NPs involves several steps.[10] First, NPs undergo opsonization, in which various proteins, such as serum albumin, complement system (CS) proteins, and immunoglobulins, adhere to the NP surface.[11] This opsonization facilitates the recognition of NPs by macrophage through specific binding interactions between the adsorbed proteins and macrophage receptors, such as the Fc receptor, complement receptor (CR), or the scavenger receptor.[12] The recognition activates a cascade of signals, leading to cytoskeleton rearrangement and the uptake of NPs into phagosomes in the macrophage. Finally, these phagosomes subsequently fuse with lysosomes, become acidified, and form enzyme-rich phagolysosomes where the internalized NPs are degraded.[13] Given that the specific binding between opsonin and receptor initiates the entire phagocytic pathway, an intervention in the initial opsonization step should be an easy and effective way to prevent the synovial macrophage phagocytosis of injected NPs and its related harmful side effects.

Within the joint microenvironment, it is still unclear how intra-articular injected NPs are phagocytosed by synovial macrophages. In this study, we first reveal that the phagocytosis for NPs by synovial macrophages is predominantly mediated by the specific binding between complement C3 (on NPs) and CD11b (on the macrophage). Once we saw the key role of C3 opsonization, we systematically evaluated the C3 adsorption by the various modified surfaces on a gelatin NPs. Zwitterionic poly(2-methacryloyloxyethyl phosphorylcholine) (PMPC) grafted as a brush layer on gelatin NPs (Gel-PMPC) most effectively suppresses C3 deposition, outperforming both cationic, anionic, and unmodified NP (**Figure 1a**). In vitro studies demonstrate that Gel-PMPC significantly inhibits C3 deposition and macrophage phagocytosis (Figure 1b), thereby efficiently inhibiting macrophage M1 polarization and the release of pro-inflammatory cytokines, as compared to NPs without the PMPC brush (Figure 1c). Moreover, in vivo experiments show that Gel-PMPC attenuates synovial inflammation, alleviates pain sensation, and protects cartilage. These results demonstrate that the novel nano-lubricant Gel-PMPC can effectively prevent macrophage-mediated clearance by blocking the initial opsonization step and restore cartilage lubrication in the OA treatment.

2. Results and Discussion

2.1. C3/CD11b Binding Mediates Synovial Macrophage Phagocytosis of NPs

After being injected into the joint cavity, NPs undergo opsonization, which facilitates their recognition and subsequent phagocytosis by synovial macrophages (**Figure 2a**). Polystyrene nanoparticles (PS-NPs) were selected as the model NPs due to their well-documented role in studying the impact on cellular interactions[11,14] (Discussion 1, Supporting Information). We co-cultured PS-NPs with mouse bone marrow-derived macrophages (BMDMs) to elucidate the mechanism by which macrophages phagocytose NPs. Confocal laser scanning microscopy (CLSM) images revealed the effective engulfment of PS-NPs by BMDMs, with intracellular colocalization of PS-NPs and lysosomes observed at 4 h (Figure S1, Supporting Information). Transcriptomic analysis of these macrophages using Kyoto Encyclopedia of Genes and Genomes (KEGG) pathway analysis (Figure 2b) and Gene Ontology (GO) analysis (Figure S2, Supporting Information) showed enrichment in pathways associated with phagocytosis, such as lysosomes, phagosomes, and endocytosis. We then specifically analyzed the expression of individual genes in phagocytosis-related pathways, and the heatmap indicated that CD11b was the most upregulated gene (Figure 2c). CD11b is a principal component of CR3, which recognizes and binds to the complement C3 on opsonized NPs, thereby facilitating macrophage-NP interactions.[15] To test whether CD11b on the synovial macrophages is regulated by the intra-articular NPs, we next co-cultured synovial tissue explants donated from OA patients with PS-NPs of various concentrations in the patient corresponding synovial fluids (simulating in vivo microenvironment) for 48 h (Figure 2d; Figure S3, Supporting Information). Immunofluorescence imaging confirmed the expression of CD11b in synovial macrophages marked with CD68 in patients with OA. Notably, PS-NPs significantly upregulated CD11b expression in synovial macrophages in a dose-dependent manner, which is consistent with the results of the transcriptomic analysis (Figure 2e,f).

We further used the human macrophage cell line THP-1 to investigate whether CD11b mediates the uptake of NPs. Prior to co-culture with THP-1 cells, the PS-NPs were opsonized for 30 min in OA patients' synovial fluids to simulate their fate in the joint's microenvironment (Figure 2g). Next, to clarify the role of CD11b in the macrophage-mediated phagocytosis for NPs, we blocked CD11b using a specific anti-CD11b antibody, with rabbit isotype IgG as a negative control. Blocking of CD11b significantly reduced the PS-NP uptake by macrophages, as shown by

X. Guo
Institute of Bast Fiber Crops
Chinese Academy of Agricultural Sciences
Changsha 410205, China

L. Wang
Department of Immunology, School of Basic Medical Sciences
Shanghai Key Laboratory of Medical Epigenetics and Metabolism
Institutes of Biomedical Sciences
Fudan University
Shanghai 200032, China

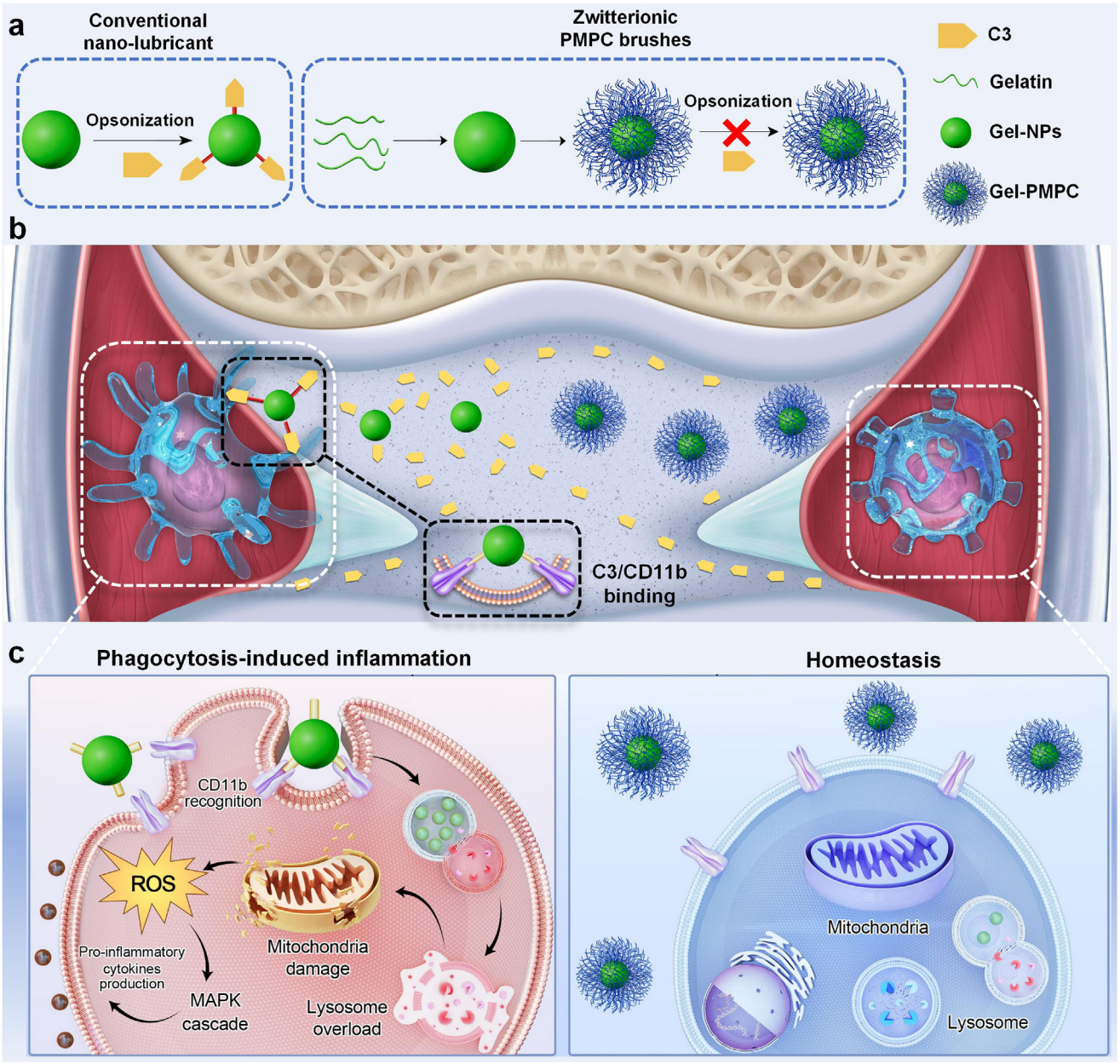

Figure 1. Gel-PMPC evades synovial macrophage phagocytosis by inhibiting C3 adsorption. a) C3 opsonization on conventional nano-lubricants initiates synovial macrophage phagocytosis within joint cavity, while Gel-PMPC can inhibit C3 opsonization on its surface. b) Gel-PMPC evades synovial macrophage phagocytosis mediated by binding of C3 (on NPs) to CD11b (on synovial macrophages). c) Excessive uptake of NPs by synovial macrophages leads to the harmful release of cytokines, inflammation, and progressive tissue injury, while Gel-PMPC maintains macrophage homeostasis by evading macrophage phagocytosis.

CLSM images and flow cytometry (FCM) (Figure 2h,I; Figure S4, Supporting Information). Similarly, CD11b knockdown using small interfering RNA (siRNA) attenuated the PS-NPs uptake (Figure 2j,k; Figures S5–S6, Supporting Information). These results confirm that CD11b is essential for macrophage-mediated NPs uptake. To determine whether the interaction between macrophages and NPs is mediated through C3/CD11b binding, we extracted adsorbed protein on opsonized NPs, and detected C3 deposition using a dot blot assay reported in literature.[16] Meanwhile, EDTA, an inhibitor of all CS pathways,[17] was introduced to synovial fluids before opsonization to terminate complement activation and suppress surface deposition on the NPs. With the addition of EDTA, the level of adsorbed C3 was reduced (Figure 2l; Figure S7, Supporting Information). Consistent with this result, THP-1 cells exhibited attenuated phagocytosis characteristics when the targeted NPs were opsonized in EDTA-containing synovial fluids. Notably, 10 mM EDTA demonstrated a stronger inhibitory effect on complement deposition and cellular phagocytosis compared to 1 mM EDTA (Figure 2m,n). Taken together, these findings demonstrate that C3 opsonization on

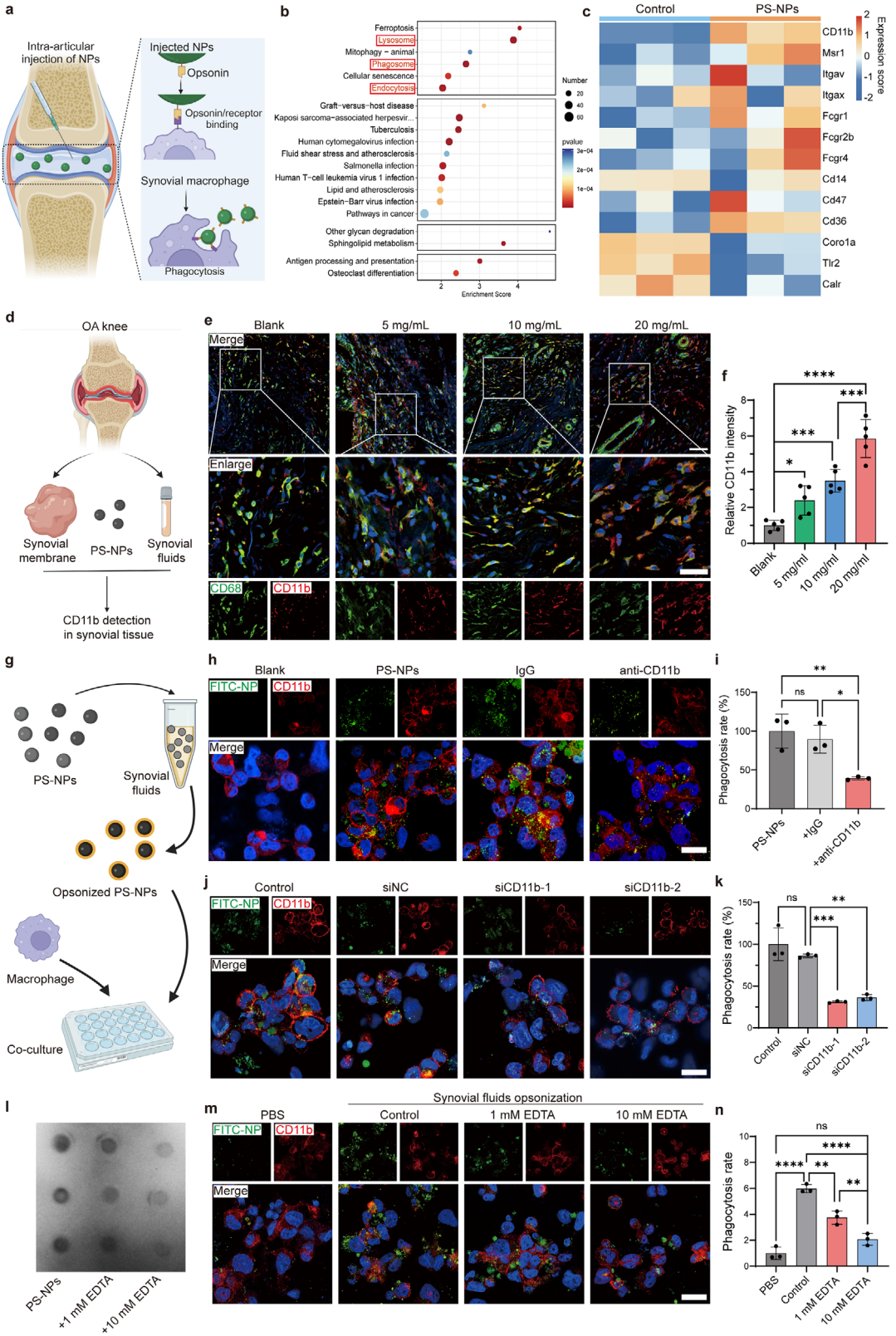

Figure 2. C3/CD11b binding mediates synovial macrophage phagocytosis for NPs. a) Schematic illustration of opsonization initiating synovial macrophage phagocytosis for injected NPs within joint cavity. b) KEGG pathway analysis and c) gene heatmap of phagocytosis-related genes in macrophage stimulated with PS-NPs for 48 h. For each group, $n = 3$ biological replications. d) Schematic illustration of CD11b detection in synovial tissue explants from OA patients after co-cultured with PS-NPs. e) Representative immunofluorescence staining images of human synovial tissue from

the NP surface and the following C3/CD11b binding are critical for macrophage recognition and phagocytosis (Supplementary Discussion 2, Supporting Information). Compared to the CD11b blockade, inhibiting C3 deposition on NPs is a more simple and effective strategy to avoid macrophage phagocytosis of injected NPs and minimize immune responses in OA therapy.

2.2. Gel-PMPC Efficiently Inhibits C3 Deposition on Its Surface

Various strategies have been explored to prevent opsonization on nanomaterials, including polymer grafting,[18] membrane cloaking,[19] and targeted regulator conjugation.[20] The most notable appears to be creating a polymer brush configuration around NPs to repel proteins adsorption.[21] Moreover, the polymer brush can act as lubricants by creating a hydration layer that reduces friction and wear between cartilage surfaces,[7a] thereby offering dual benefits by providing lubrication to reduce joint friction while also modulating immune responses. Therefore, we designed three nano-sized spherical brushes by grafting cationic (poly-methacrylatoethyl trimethyl ammonium chloride, PMETAC), anionic (poly-acrylic acid, PAA), or zwitterionic (PMPC) polymer brush from the surface of a gelatin core particle (Gel-NPs); the products are denoted as Gel-PMETAC, Gel-PAA, and Gel-PMPC, respectively (**Figure 3**a; Figure S8, Supporting Information). NMR, X-ray photoelectron spectroscopy (XPS), and Fourier transform infrared (FTIR) analysis verified the successful grafting of polymers onto the gelatin cores (Figure 3b–e; Figures S9,S10, Supporting Information). The average hydrodynamic diameters of the products were measured using dynamic light scattering (DLS), with the lengths of the three different brushes controlled to approximately the same value (≈140 nm) (Figure S11, Supporting Information).

To ascertain which spherical brush can efficiently inhibit C3 adsorption, we opsonized these NPs in synovial fluids and again used dot blot assay to detect the deposited C3 on their surfaces. The C3 deposited on three NPs with spherical brushes was significantly decreased compared to naked PS-NPs and Gel-NPs, and the PMPC brush exhibited maximum inhibition of C3 adsorption on NPs (Figure 3f,g; Discussion 3, Supporting Information). To further characterize C3 deposition on different NPs, we semi-quantified C3 adsorption at multiple time points (Figure S12, Supporting Information), suggesting that Gel-PMPC consistently exhibits the lowest C3 adsorption over time. Zeta potential measurements were conducted to evaluate the surface charge of different NP formulations. The strong charges of Gel-PMETAC and Gel-PAA likely promote C3 adsorption, while the near-neutral charge of Gel-PMPC, along with its zwitterionic hydration layer, minimizes C3 binding via less electrostatic interactions and a stable hydration layer (Figure S13, Supporting Information). Consistently, macrophage phagocytosis assays revealed that NPs with higher C3 deposition exhibited increased uptake by THP-1 macrophages, while Gel-PMPC, with the lowest C3 adsorption, showed minimal phagocytosis (Figure S14 and Discussion 4, Supporting Information), further confirming the role of C3 in complement-mediated uptake.

Because the length of polymer chains may also influence the protein adsorption, we prepared Gel-PMPC with short (Gel-PMPC-S), medium (Gel-PMPC-M), and long (Gel-PMPC-L) PMPC brush and compared the quantity of adsorbed C3 on their surfaces. Both Gel-PMPC-M and Gel-PMPC-L showed better inhibition for C3 adsorption compared to Gel-PMPC-S, while no significant difference were observed between them (Figure 3h,i). Moreover, Gel-PMPC-M and Gel-PMPC-L exhibited better lubrication than short-chain Gel-PMPC, with no significant difference between the medium and long chains (Figure S15, Supporting Information). Based on these findings, we select Gel-PMPC with medium polymer brush to demonstrate subsequent experiments (Discussion 5, Supporting Information). PMPC is a biomimetic lubricant molecule which reduces friction in joint motion.[7a,22] The lubricating properties of Gel-PMPC were examined using trypsin-treated isolated porcine cartilage, as well as human articular cartilage donated by OA patients, by means of static and kinetic friction coefficients. We employed a rheometer to assess the lubrication performance of Gel-PMPC, a method widely used in biological lubrication studies.[7a,23] Gel-PMPC demonstrated superior lubrication properties at higher concentration (Figure S16, Supporting Information). Besides, DLS measurements were performed at 3 days, 1 week, and 2 weeks post-incubation in OA patient-derived synovial fluid. The hydrodynamic diameter remained stable with no significant aggregation (Figure S17, Supporting Information), confirming excellent colloidal stability.

Although PMPC-modified NPs have been shown to escape macrophage phagocytosis for treating OA,[24] the mechanism underlying this behavior still remains unclear. We hypothesized that PMPC brush can efficiently evade synovial macrophage recognition and phagocytosis by inhibiting C3 opsonization within joint cavity. Given that softer NPs show a lower phagocytosis rate than stiffer NPs,[25] we selected gelatin as the core material because it can be softened by matrix metalloproteinases (MMPs)[26] in the OA microenvironment. To determine whether particle softening

OA patients after co-culturing with PS-NPs at different concentrations for 48 h. $n = 5$ biologically independent patients for each group. Green, CD68; red, CD11b; blue, DAPI. Scale bars, 100 μm (top lane), 40 μm (bottom lane). f) Quantitative results for the CD11b in CD68+ macrophage in the synovium (n = 5 biologically independent samples). g) Schematic illustration of opsonization of NPs in synovial fluids and the subsequent co-culturing. h) Immunofluorescence staining images of THP-1 cells phagocytoses FITC-NP with CD11b blockade. Green, FITC-labeled PS-NPs; red, CD11b; blue, DAPI. Scale bars, 10 μm. i) Quantitative results for FITC-NPs in THP-1 cells (n = 3 independent samples). j) Immunofluorescence staining images of THP-1 cells phagocytoses FITC-NP with CD11b knockdown. Green, FITC-labeled PS-NPs; red, CD11b; blue, DAPI. Scale bars, 10 μm. k) Quantitative results for FITC-NPs in THP-1 cells (n = 3 independent samples). l) Dot blot assay of deposited C3 on PS-NPs with or without EDTA addition after opsonization in synovial fluids. m) Immunofluorescence staining images of THP-1 cells after phagocytosis for FITC-NPs. EDTA was added to end the activation of CS. Green, FITC-labeled PS-NPs; red, CD11b; blue, DAPI. Scale bars, 10 μm. n) Quantitative results for FITC-NPs in THP-1 cells (n = 3 independent samples). Data were analyzed using one-way analysis of variance (ANOVA) with Tukey's post hoc test, and are shown as mean ± standard deviation (s.d.). $*p < 0.05$, $**p < 0.01$, $***p < 0.001$, and $****p < 0.0001$. Schematic illustrations were created with Biorender.com.

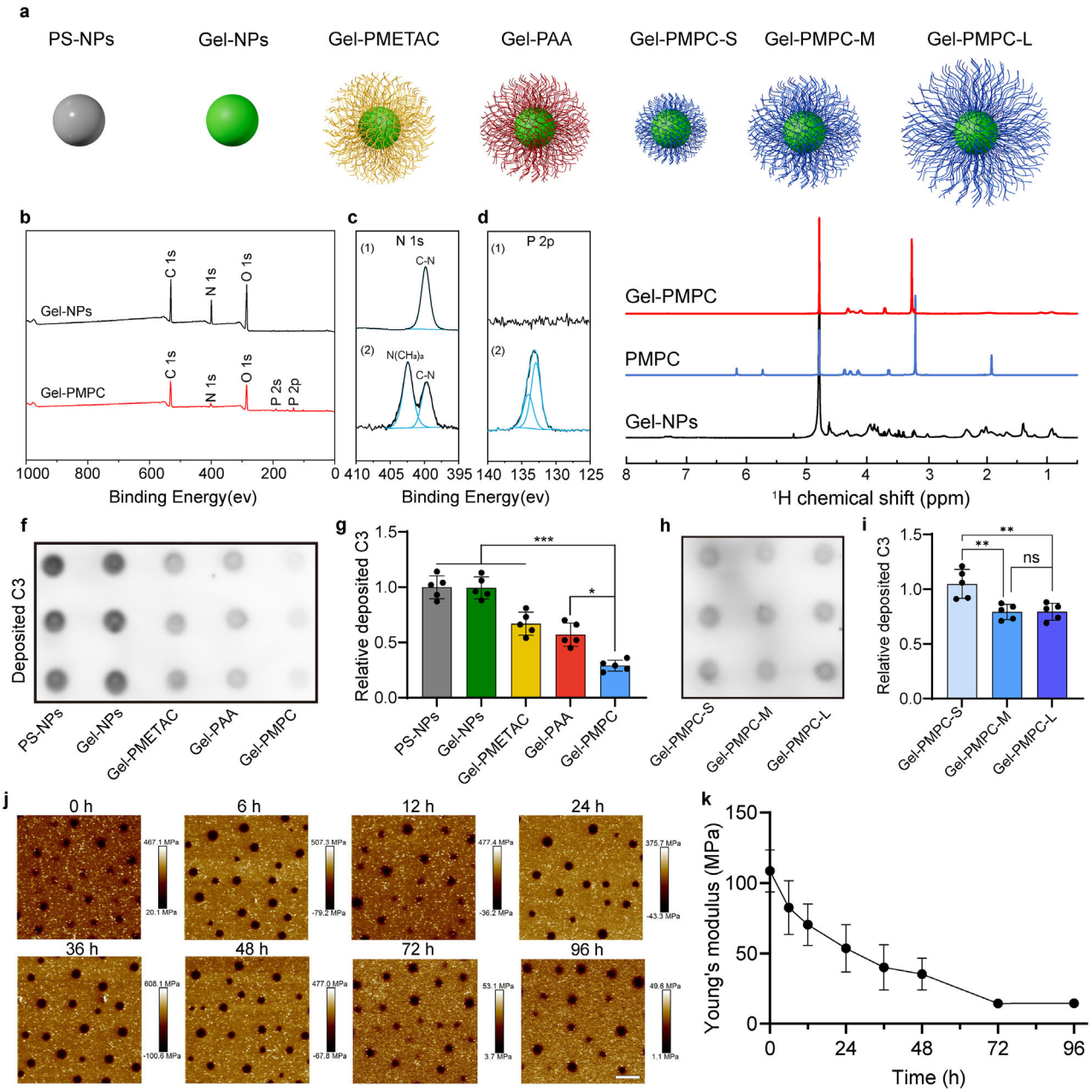

Figure 3. Synthesis and characterization of nano-sized spherical brushes. a) Schematic illustration of naked PS-NPs, Gel-NPs, and nano-sized spherical brushes. b–d) XPS characterization of Gel-NPs and Gel-PMPC. b) Survey spectra of Gel-NPs and Gel-PMPC and c) the high- resolution spectra of N 1s and d) P 2p for Gel-NPs (1) and Gel-PMPC (2). In the XPS spectrum of Gel-NPs, only signals corresponding to C, O, and N were detected. After the grafting of PMPC brush, new signals for P 2s and P 2p appeared at 190 and 133 eV, respectively. Additionally, a new N 1s peaks appeared at 402 eV, attributed to the quaternary ammonium group in PMPC (c). The high-resolution P 2p spectrum further confirmed the successful grafting of PMPC brush onto the Gel-NPs (d). e) ^{1}H NMR spectrum of Gel-NPs, PMPC, and Gel-PMPC. f) Dot blot assay and g) relative level of deposited C3 on different NPs after opsonization in synovial fluids. h) Dot blot assay and i) relative level of deposited C3 on Gel-PMPC with different length of PMPC after opsonization in synovial fluids. j) Representative AFM images indicating the softening process of Gel-PMPC due to the enzymatic attack by MMP-13 (100 ng mL^{-1}). Scale bars, 2 μm. k) Young's modulus of Gel-PMPC in MMP-13 solutions to simulate OA environment over time (n = 5 independent samples). Data were analyzed using one-way ANOVA with Tukey's post hoc test and are shown as mean ± s.d.

occurred, Gel-PMPC was immersed in MMP-13 solutions mimicking the OA microenvironment. The concentration of MMP-13 in the solution was determined based on the levels found in the synovial fluid of patients with OA. Mechanical testing using atomic force microscopy (AFM) confirmed that MMP-13 reduced the stiffness (Young's modulus) of Gel-PMPC by ≈60% after 96 h of incubation (Figure 3j,k), whereas PMPC-grafted PS-based NPs (PS-PMPC) showed no change in stiffness (Figure S18 and Discussion 6, Supporting Information). Enzymatic softening of the core would contribute to the immune escape of

Gel-PMPC by helping it evade synovial macrophage phagocytosis. Transmission electron microscopy (TEM) images of Gel-NPs and Gel-PMPC before and after MMP-13 treatment were captured for 72 h (Figure S19, Supporting Information). Dynamic lubrication tests of Gel-NPs and Gel-PMPC were performed after MMP-13 treatment at different time points (Figure S20, Supporting Information). Even after treatment with MMP-13, Gel-PMPC still maintained its superior lubrication effect, suggesting that the enzymatic attack by MMPs did not affect the lubrication properties of Gel-PMPC because they only attack the core and do not impact the PMPC brush.

2.3. Gel-PMPC Evades Macrophage Phagocytosis by Inhibiting C3 Opsonization

We assumed that the PMPC brush contributed to the evasion of synovial macrophage phagocytosis by the NPs (**Figure 4a**). Gel-PMPC was incubated in the synovial fluid of patients with OA, with naked Gel-NPs as a control. Scanning electron microscopy (SEM) images showed that naked Gel-NPs aggregated in the synovial fluid, whereas Gel-PMPC particles remained colloidally stable with less aggregation (Figure S21, Supporting Information). The DLS and zeta potential measurements were consistent with the SEM findings (Figure S22, Supporting Information). CLSM confirmed that the PMPC brush significantly inhibited the deposition of C3 on the Gel-PMPC surface; less C3 was detected by Alexa Fluor 647 (AF647)-labeled C3 antibody on the surface of Gel-PMPC (Figure 4b). To quantify the deposited C3 on the surfaces of Gel-NPs and Gel-PMPC, we washed the opsonized NPs and performed western blot analysis under reducing conditions, as described previously (Figure 4c).[27] The amounts of bound C3 and its cleavage products on Gel-PMPC were lower than those on naked Gel-NPs, (Figure 4d,e), suggesting that the zwitterionic PMPC brush could effectively inhibit C3 opsonization on NP surfaces.

Next, we explored whether the inhibition of C3 deposition contributes, as expected, to evading macrophage phagocytosis. After opsonization in synovial fluids, different NPs were co-cultured with THP-1 cells for 4 h (Figure 4c). The CLSM images and FCM quantified analysis showed that fewer NPs were observed in THP-1 cells treated with Gel-PMPC, than in those treated with Gel-NPs and PS-PMPC (Figure 4f–h). Consistent with our findings, previous work has shown that zwitterionic coatings can significantly reduce immune recognition and macrophage uptake, supporting the rationale of using PMPC to enhance immune evasion and therapeutic retention.[28] To further investigate the role of C3 in macrophage-mediated phagocytosis, we performed in vitro experiments using C3 neutralizing antibody and Compstatin (C3 convertase inhibitor) to selectively inhibit C3 activity in OA synovial fluid for the opsonization (Figure S23, Supporting Information). Before C3 inhibition, Gel-NPs exhibited significantly higher phagocytosis than Gel-PMPC. However, after C3 inhibition, the phagocytosis rate of Gel-NPs decreased dramatically, while Gel-PMPC showed minimal changes in phagocytosis. Collectively, these data demonstrate that PMPC brush plays a major role in evading macrophage phagocytosis, not only by inhibiting the access of C3 to the NP surface, but also by the enzymatic softening of the gelatin core.

2.4. Gel-PMPC Inhibits M1 Macrophage Polarization and Pro-Inflammatory Cytokines Release

It has been reported that the uptake of foreign particles will polarize macrophage from a "resting" state to an activated state.[29] M1 macrophage secretes many pro-inflammatory cytokines including interleukin (IL)-1β, IL-6, and tumor necrosis factor (TNF)-α, leading to the degradation of cartilage matrix and OA progression[30] (**Figure 5a**). To investigate the immune responses induced by NPs, we treated synovial tissue explants with different opsonized NPs and observed the phenotypic transformation of the synovial macrophages, as well as subsequent production of pro-inflammatory cytokines. M1 synovial macrophages were identified using the specific marker CD86. The fraction of M1 macrophages in the explants treated with Gel-PMPC was significantly lower than that in the explants treated with Gel-NPs and PS-PMPC, whereas the M1 fractions in the Control and Gel-PMPC groups were comparable (Figure 5b,c). Consistent with the M1 polarization data, less production of pro-inflammatory cytokines was detected in the synovial tissue treated with Gel-PMPC, as compared to other NPs (Figure 5d–f). Similar to the data from synovial explants, the THP-1 cells treated with Gel-PMPC showed significantly lower ratio of M1 macrophages (Figures S24,S25, Supporting Information) and less production of these pro-inflammatory cytokines than those treated with Gel-NPs and PS-PMPC (Figure S26, Supporting Information). These data underscore the importance of the PMPC brush in preventing M1 macrophage polarization and reducing the production of pro-inflammatory cytokines in the OA microenvironment.

Next, we explored the mechanisms underlying M1 macrophage polarization and proinflammatory cytokine production after NPs opsonization. Studies have indicated that the uptake of NPs can induce the generation of reactive oxygen species (ROS),[31] and the elevated levels of ROS in macrophages disrupt mitochondrial energy metabolism, promoting the secretion of inflammatory factors.[32] As the Gene Set Enrichment Analysis (GSEA) confirmed the oxidative stress and inflammatory response after treatment with PS-NPs (Figures S27,S28, Supporting Information), we analyzed the ROS level and the mitochondrial membrane potential (Ψm) in THP-1 cells treated with different NPs. Macrophages treated with Gel-PMPC exhibited weaker ROS generation (Figure S29, Supporting Information) and less mitochondrial membrane disruption (Figure S30, Supporting Information) than macrophages treated with Gel-NPs and PS-PMPC. In addition, WikiPathways enrichment analysis suggested that the uptake of PS-NPs upregulated the mitogen-activated protein kinases (MAPK) signaling pathway (Figure S31, Supporting Information), which might promote M1 macrophage polarization and pro-inflammatory cytokines secretion as well.[33] The expression of several proteins within the MAPK pathway was examined to test whether NP uptake polarized the M1 macrophages by activating the MAPK cascade. No significant upregulation was observed in the phosphorylation (p-) levels of p38, ERK, and JNK in macrophages treated with Gel-PMPC compared with those in the control group (Figure 5g,h). Collectively, these results confirm that the strongly reduced engulfment of Gel-PMPC effectively prevents ROS generation, mitochondrial disruption, and the upregulation of the MAPK

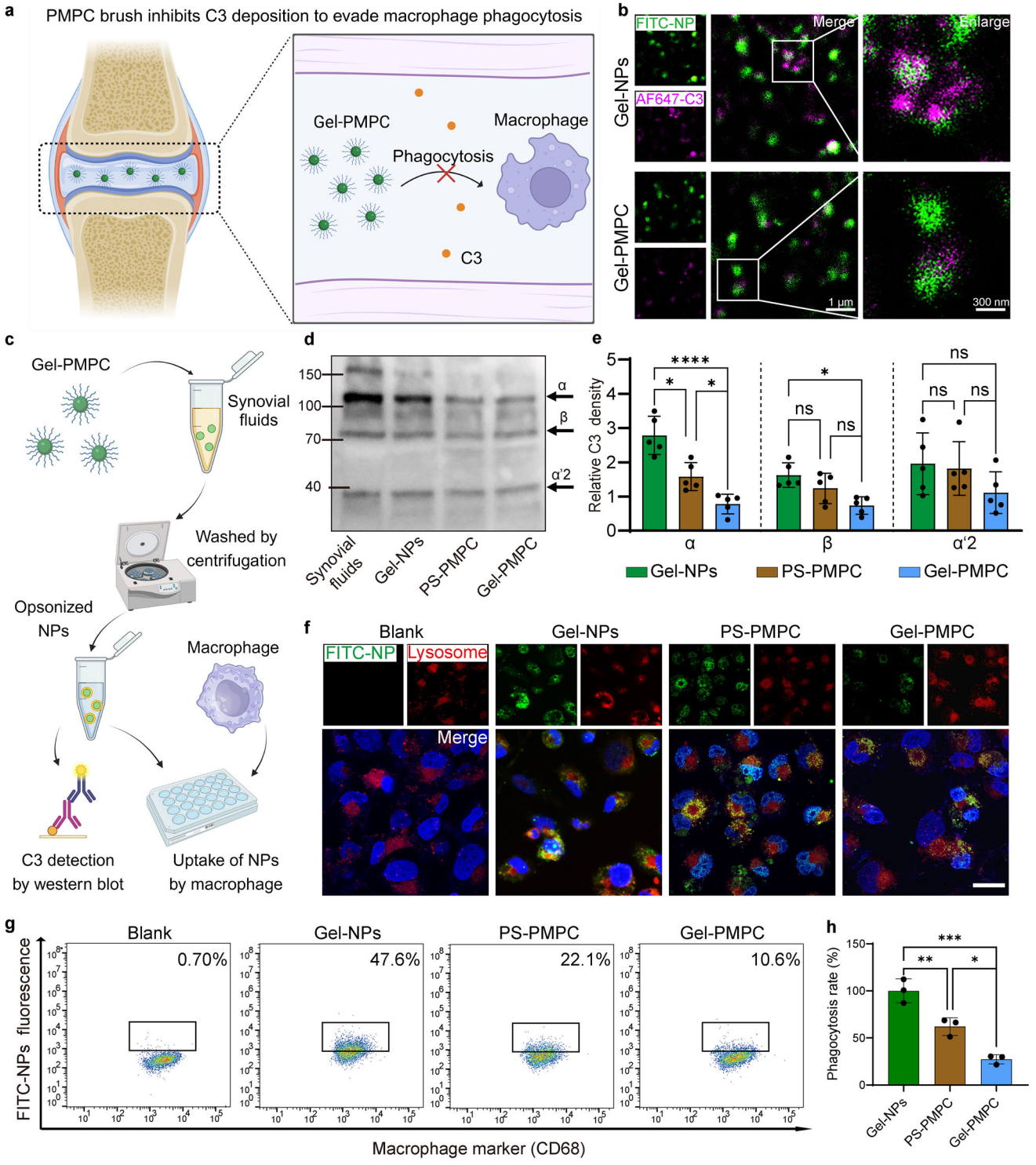

Figure 4. Gel-PMPC evades macrophage phagocytosis by inhibiting C3 adsorption to its surface. a) Schematic illustration of Gel-PMPC evading synovial macrophage phagocytosis in joint cavity. b) Representative images of FITC-labeled Gel-NPs or Gel-PMPC and the deposited C3 detected by AF647 labeled-C3 antibody. Scale bars, 1 μm (left), 300 nm (right). c) Schematic illustration of the opsonization of NPs in synovial fluids for further C3 assessment and cellular uptake. d) Detection of deposited C3 on different NPs in human synovial fluids through western blot analysis. α-chain (115 kDa), β-chain (75 kDa), and α'2 (43 kDa) on the particles were detected by C3 antibody. E) Relative C3 level deposition on NPs analyzed by western blot experiments compared with diluted synovial fluids ($n = 5$ independent samples.). f) Representative images of the uptake and intracellular distribution of FITC-labeled Gel-NPs, PS-PMPC, or Gel-PMPC in THP-1 cells. Green, FITC-labeled NPs; red, Lysosome; blue, DAPI. Scale bars, 20 μm. g) Representative FCM results and h) phagocytosis rate of THP-1 cells co-cultured with opsonized FITC-NPs after incubation for 4 h ($n = 3$ per group). Data were analyzed using two-way (e) or one-way (h) ANOVA with Tukey's post hoc test, and are shown as mean ± s.d. *$p < 0.05$, **$p < 0.01$, ***$p < 0.001$, and ****$p < 0.0001$. Schematic illustrations were created with Biorender.com.

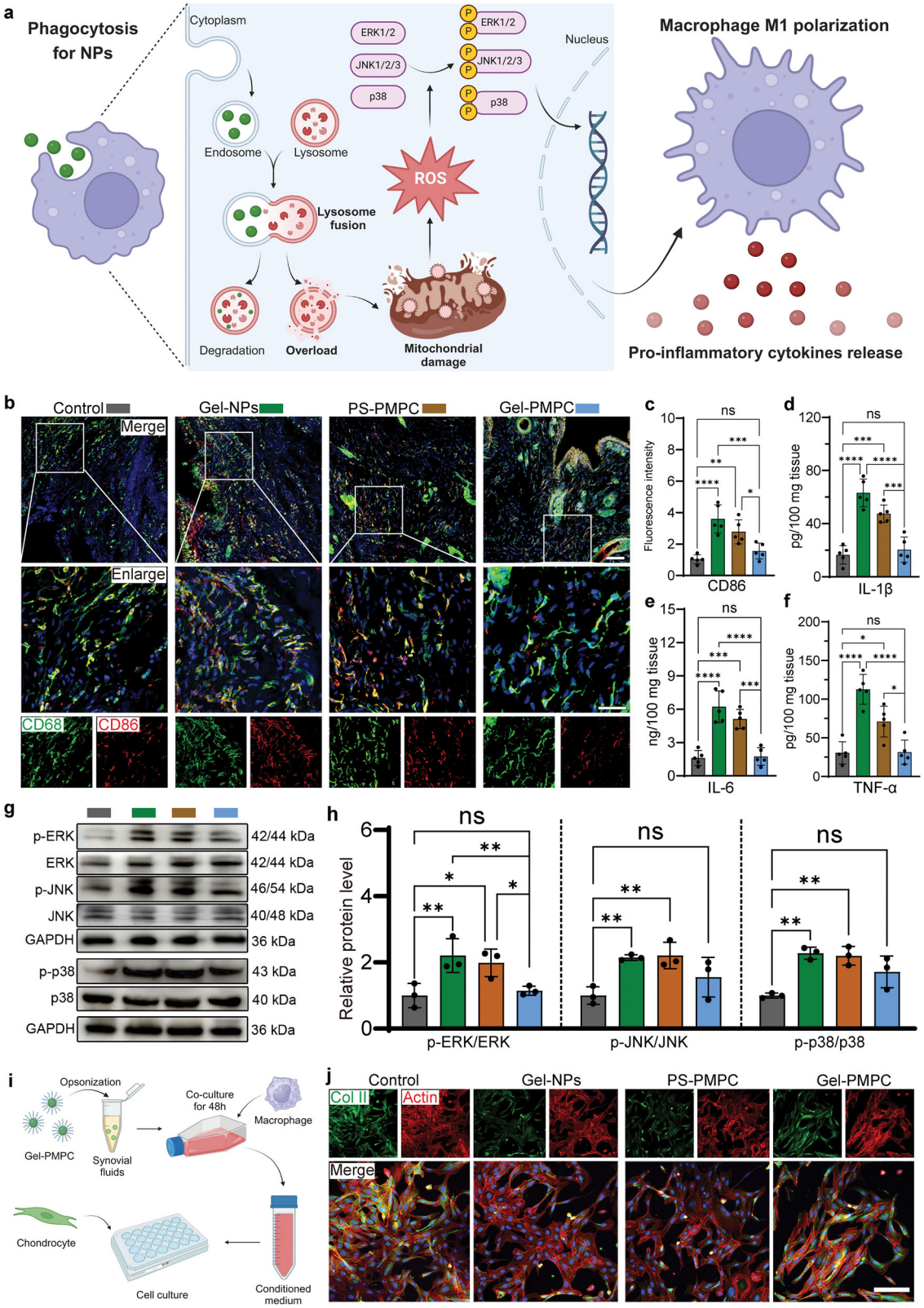

Figure 5. Gel-PMPC inhibited macrophage M1 polarization and pro-inflammatory cytokines release. a) Schematic illustration of the uptake of NPs leading to lysosome overload, mitochondrial damage, ROS generation, and MAPK pathway activation. These processes ultimately result in macrophage polarization and the release of pro-inflammatory cytokines. b) Representative images of immunofluorescence staining of human synovial tissue from OA patients after co-culturing with different NPs for 48 h. Green, CD68; red, CD86; blue, DAPI. Scale bars, 100 μm (top lane), 50 μm (bottom lane).

signaling pathway, thereby reducing the inflammatory response induced by foreign particles.

The crosstalk between chondrocytes and synovial macrophages amplifies the inflammatory response and cartilage degradation in OA.[34] Pro-inflammatory cytokines released by synovial macrophages stimulate chondrocytes to produce enzymes that degrade the cartilage matrix, which further induces macrophage activation and more pro-inflammatory cytokines release.[35] Hence, it is essential to avoid primary macrophage activation in the intra-articular applications of NPs. To evaluate the possible interactions between NP-engulfed macrophages and chondrocytes, the human chondrocyte cell line C28/I2 was cultured in conditioned medium collected from macrophages treated with different NPs (Figure 5i). As shown in the CLSM images, the Gel-PMPC group exhibited higher collagen II (Col II, a major component of the cartilage matrix secreted by chondrocytes) expression than the other NPs groups, due to the reduced release of pro-inflammatory cytokines (Figure 5j). This was confirmed by the increased mRNA levels of other chondrogenic markers, including SOX-9 and aggrecan, detected by Quantitative Real-time Polymerase Chain Reaction (qPCR) (Figure S32, Supporting Information). In summary, these data indicate that Gel-PMPC has a minimal influence on macrophage-chondrocyte crosstalk in the OA microenvironment.

2.5. In Vivo Therapeutic Effects of Gel-PMPC in Rat Models of OA

Before proceeding to in vivo studies, we investigated whether Gel-PMPC exhibited good biocompatibility. C-28/I2 cells treated with different concentrations of Gel-PMPC were evaluated using the live/dead and cell counting kit-8 (CCK-8) assays, and the results indicated that Gel-PMPC had no significant influence on cell viability (Figure S33, Supporting Information). Moreover, 4 weeks after the intra-articular injection of Gel-PMPC, no obvious tissue damage was detected of the major organ of the rats (Figure S34, Supporting Information). Blood cell counts and routine hematological indicators of liver and kidney function remained within normal ranges across all groups, with no significant differences observed (Figure S35, Supporting Information). These results reveal that Gel-PMPC does not induce systemic toxicity. The therapeutic effect of Gel-PMPC for the prevention of OA was evaluated in vivo by a well-characterized surgically induced rodent OA model, in which the rats were subjected to right anterior cruciate ligament transection (ACLT). The retention time of Gel-PMPC in the joint cavity was at least 14 days, which is considerably longer than Gel-NPs and PS-PMPC (Figure S36, Supporting Information). This suggests that the ability of Gel-PMPC to evade macrophage-mediated phagocytosis contributes to its extended retention in the joint cavity. Four weeks after the surgical introduction of OA, the rats received intra-articular injections twice a week and were separated into five groups: Saline, Gel-NPs, PS-PMPC, Gel-PMPC, and a sham group (**Figure 6**a).

After 8 weeks of treatment, all rats survived without signs of infection and were subsequently tested and sacrificed. Given that OA is accompanied by progressive gait disturbances and pain, we first collected gait kinematic parameters that reflected the severity of joint instability and pain. Foot contacts of rats in each group disrupted the optical effect, leading to light scattering detected by a high-speed camera (Figure 6b). The paw pressure data, including print area and contact intensity, were collected. The results show that the Saline group had reduced pressure on the right foot, similar to the Gel-NPs and PS-PMPC groups. In contrast, the rats injected with Gel-PMPC performed closely to baseline values of the sham group, indicating effective pain attenuation in their OA knee (Figure 6c). As OA progressed, the rats were reluctant to bear weight on the affected paw due to pain, leading to a smaller pawprint area and less contact intensity. Gel-PMPC alleviates pain by reducing friction between the surfaces of the joints owing to its superlubricating property. The immune escape behavior of Gel-PMPC contributes to prolonged retention time and reduced inflammation in the joint cavity, thereby protecting cartilage from degeneration.

OA is characterized by osteophyte (bone spur) formation and subchondral bone remodeling.[36] Therefore, we next evaluated the bone response using micro-computer tomography (micro-CT) (Figure 6d). The osteophyte volumes of all four treatment groups were significantly increased, compared to the sham-operated group, i.e., Saline group (5.94 ± 1.00 mm^3), Gel-NPs (5.67 ± 0.99 mm^3), PS-PMPC (4.36 ± 0.72 mm^3), and Gel-PMPC (2.51 ± 0.77 mm^3). Notably, osteophyte volume in the Gel-PMPC group was significantly lower than that in the saline group (Figure 6e). Moreover, images of subchondral bones were digitally reconstructed (Figure 6f), and the ratio of bone volume to tissue volume (BV/TV) was calculated to assess the extent of remodeling. The Gel-PMPC group showed no obvious abnormal changes, similar to those in the healthy sham-operated group (Figure 6g). Compared with the Saline group, Gel-PMPC showed a statistically significant decrease in BV/TV (62.93 ± 4.59% to 56.01 ± 3.88%), which were nearly equiv. to the sham-operated group (50.97 ± 3.51%), indicating that the injection of Gel-PMPC effectively ameliorates subchondral osteosclerosis in the rat model of OA. High friction causes articular cartilages to rub against each other, resulting in bone remodeling and restricted joint motion.[37] In our study, the injection of Gel-PMPC restored lubrication to avoid direct contact with the cartilage, thus effectively attenuating the bone response in OA.

Damage and degeneration of the articular cartilage is another major pathological feature of OA.[38] We assessed the changes in the articular cartilage through histological analysis. In Safranin O-fast green (SO&FG) cartilage-distinguishing staining,

c) Quantitative results for the CD86 in macrophage in the synovium (n = 5 independent samples). d–f) The secretion of d) IL-1β, e) IL-6, and f) TNF-α from synovial explants per 100 mg tissue, test by ELISA assay (n = 5 biologically independent samples). g,h) Expression of proteins in MAPK signaling pathway detected by g) western blot analysis and h) quantitative results of the ratio of p-ERK/ERK, p-JNK/JNK, and p-p38/p38 (n = 3 biologically independent samples). i) Schematic illustration of experiments on the crosstalk between THP-1 cells and C28/I2 chondrocytes. j) Immunofluorescence staining of Col II (green) and actin (red) of C28/I2 cells cultured with conditioned medium collected from macrophage treated with different NPs. Green, Col II; red, actin; blue, DAPI. Scale bars, 100 µm. Data were analyzed using one-way ANOVA with Tukey's post hoc test, and are shown as mean ± s.d. *p < 0.05, **p < 0.01, ***p < 0.001, and ****p < 0.0001. Schematic illustrations were created with Biorender.com.

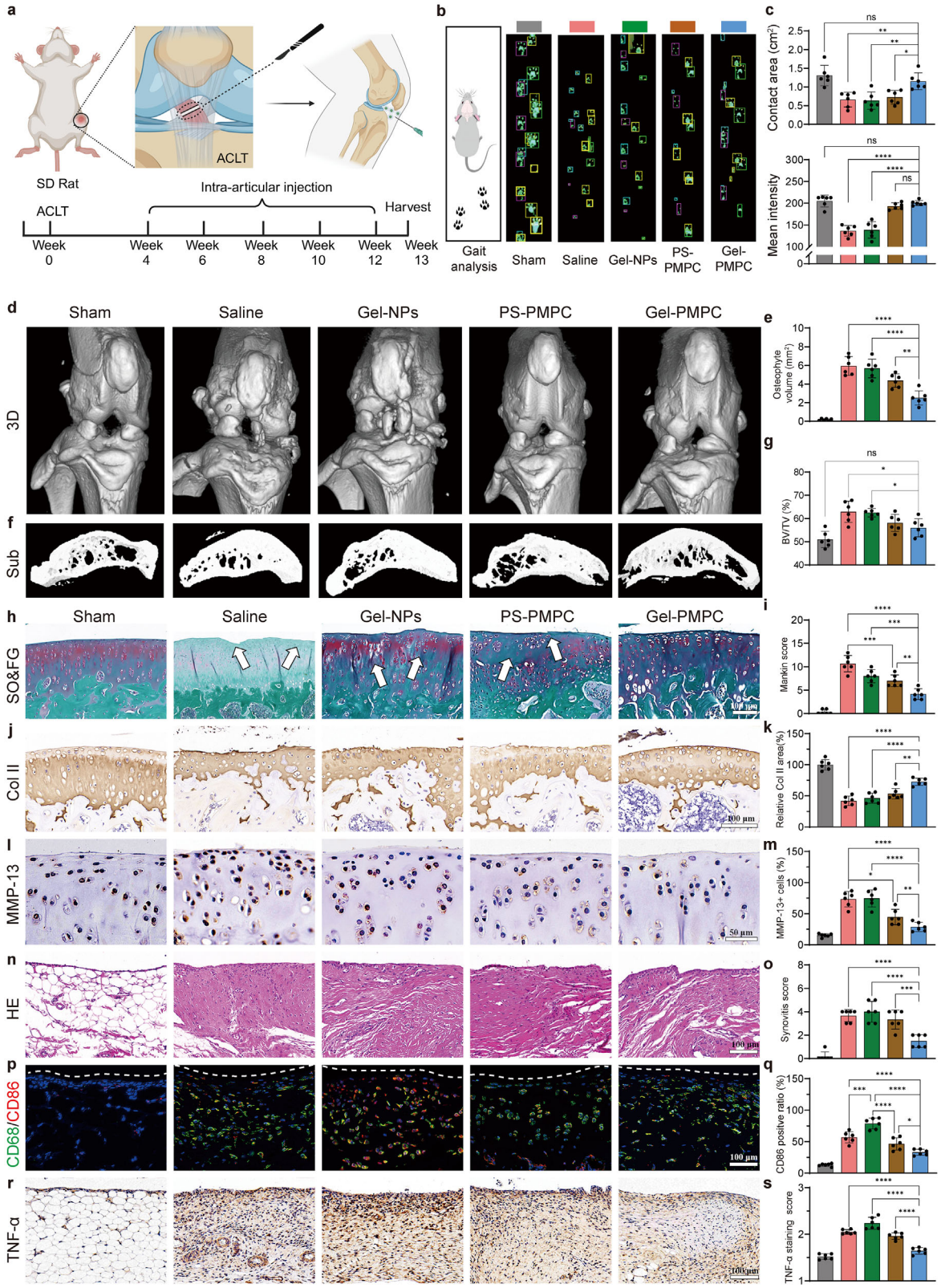

Figure 6. Gel-PMPC treatment attenuates OA development in rat models. a) Schematic illustration of a rat knee coronal section exhibiting the ACLT surgery (top) and timeline of different treatments for surgery-induced OA rats (bottom). b) The pawprint pressure heat map of rats in each group. Yellow box is the gait of the limb in each rat. c) Contact area and max intensity of right limb assessed by catwalk system ($n = 6$ biologically independent rats). d) Representative image of 3D reconstruction of sequential frontal slices showing the surface morphology of the joints. e) Total osteophyte volume

the saline group showed cartilage erosion, disorganized structure, and weak staining. In contrast, these degenerative changes significantly reduced in the Gel-PMPC group (Figure 6h; Figure S37, Supporting Information). Mankin score was employed to evaluate the severity of cartilage degeneration. The Mankin score of the Gel-PMPC group (4.17 ± 1.17) was significantly lower than the Saline group (10.67 ± 1.75), the Gel-NPs group (8.00 ± 1.41), and the PS-PMPC group (7.00 ± 1.26) (Figure 6i). The Mankin score of the Gel-PMPC group was significantly lower than that of the saline group. Considering that Col II serves as a marker of cartilage health, whereas MMP-13 indicates cartilage degradation,[39] we analyzed both Col II and MMP-13 protein expression in the cartilage by immunohistochemistry. The Gel-PMPC group exhibited a significantly higher expression of Col II (Figure 6j,k) and lower expression of MMP-13 (Figure 6l,m) compared to the Saline group. The behavior of chondrocytes is highly regulated by load and pressure.[40] Increased friction between articular cartilages in OA leads to higher shear stress on the cartilage surface, causing upregulation of catabolic cartilage-degrading enzymes via mechanical transduction of the cell.[6a] Our results confirmed that Gel-PMPC can reduce friction and shear stress at the cartilage interface, thereby providing chondroprotection. More importantly, the macrophage-evading property of the PMPC brush enhanced the bioavailability of this nanolubricant and prevented potential-induced inflammation, allowing it to perform its function longer and more effectively.

It has been reported that particles associated with joint implants, phagocytosed by synovial macrophages, lead to the polarization of the latter to the M1 phenotype and to the release of pro-inflammatory cytokines.[41] To investigate whether Gel-PMPC can avoid these side effects by evading macrophage phagocytosis, we examined the severity of inflammation, the M1 macrophage profile, and the expression of pro-inflammatory cytokines in the synovial tissue. Hematoxylin and eosin (H&E) staining was performed to evaluate synovial inflammation using a semiquantitative scoring system based on the guidelines provided by the Osteoarthritis Research Society International (OARSI)'s histopathology initiative.[42] Compared to the Gel-NPs and PS-PMPC groups, the Gel-PMPC group displayed a remarkably decreased number of inflammatory cells and reduced synovitis score (Figure 6n,o). Furthermore, the Gel-PMPC group exhibited a significantly lower M1 (CD68 +)/total macrophage (CD86 +) ratio in the synovial tissue than the Gel-NPs and PS-PMPC groups (Figure 6p,q). Moreover, the expression of TNF-α, one of pro-inflammatory cytokines, was examined in synovial tissue by immunohistochemistry, and we found that less TNF-α was secreted in the Gel-PMPC group than in the Gel-NPs and PS-PMPC groups (Figure 6r,s). Taken together, these results confirmed that Gel-PMPC can prevent inflammatory side effects by evading macrophage phagocytosis.

Although administering lubricants (e.g., hyaluronic acid) seems a plausible approach to relieve pain for OA patients, conflicting clinical reports raise doubts about their efficacy.[43] We now understand that this may occur because synovial macrophages tend to capture the injected lubricants, thereby weakening their therapeutic effect as well as provoking a harmful immune response. Moreover, through systematically demonstrating that C3 plays a pivotal role in macrophage-mediated NPs clearance in OA synovial fluid, our study extends beyond previous research by providing direct mechanistic evidence linking C3 opsonization to PMPC-mediated immune evasion, rather than solely attributing it to protein-repelling properties. Furthermore, we highlight the dual-functional role of PMPC in OA therapy by integrating complement inhibition with enhanced joint lubrication, thereby offering a novel strategy for OA treatment.

3. Conclusion

OA treatment with just a conventional nano-lubricant is not sufficient: the nano-lubricant must also be able to avoid macrophage phagocytosis. In this study, we established that the clearance of intra-articular injected NPs is mediated by the specific binding of C3 (on NPs) to CD11b (on synovial macrophages). Having understood this key role of C3/CD11b binding in synovial macrophage phagocytosis, we developed nano-sized gelatin particles carrying a PMPC brush (Gel-PMPC), with not only superior lubricity but also a low affinity for C3, allowing for (1) evasion of synovial macrophage phagocytosis, (2) avoidance of macrophage M1 polarization, and (3) prevention of the release of harmful cytokines in the OA microenvironment. Overall, our strategy offers an effective approach to treat OA with two benefits: optimizing lubrication and reducing macrophage phagocytosis and inflammation, which may be promising in the future.

4. Experimental Section

Materials: Human THP-1 cell line (ZQ0086) was purchased from ZQXZ-bio. Human chondrocyte C28/I2 cell line (SCC043) was obtained from Sigma-Aldrich. Lyso-Tracker Red (C1046), Calcein/PI Cell Viability/Cytotoxicity Assay Kit (C2015S), CCK-8 (C0037), Insulin-Transferrin-Selenium Media Supplement (ITS, C0341), L-proline (ST1500), ROS Assay Kit (S0033S), Enhanced mitochondrial membrane potential assay kit with JC-1 (C2003S) and Triton X-100 (P0096) were obtained

of each joint was quantified (n = 6 biologically independent rats). f) Reconstructed subchondral bone images micro-CT images (n = 6 biologically independent rats). g) The BV/TV of tibial subchondral bone microarchitecture was quantified (n = 6 biologically independent rats). h) Representative images of SO&FG staining of the operated knee joints after injected NPs treatments. White arrows indicate the damaged or degenerated articular cartilages. Scale bar, 100 μm. i) The severity of cartilage degeneration was evaluated by Mankin score in each group (n = 6 biologically independent rats). j) Representative images and k) quantitative analysis of immunohistochemical staining of Col II in the articular cartilage after the treatments. Scale bar, 100 μm (n = 6 biologically independent rats). l) Representative images and m) quantitative analysis of immunohistochemical staining of MMP-13 in the articular cartilage after the treatments. Scale bar, 50 μm (n = 6 biologically independent rats). n) Representative images of H&E staining and o) synovitis score in the synovial tissue. Scale bar, 100 μm. (n = 6 biologically independent rats). p) Representative images of immunofluorescence staining and q) the ratio of CD86/CD68 in the synovial tissue. Scale bar, 100 μm (n = 6 biologically independent rats). r) Representative images and s) quantitative analysis of immunohistochemical staining of TNF-α in the synovial tissue. Scale bar, 100 μm (n = 6 biologically independent rats). Data were analyzed using one-way ANOVA with Tukey's post hoc test, and are shown as mean ± s.d. *p < 0.05, **p < 0.01, ***p < 0.001, and ****p < 0.0001. Schematic illustrations were created with Biorender.com.

from Beyotime Biotechnology. Cell culture-related reagents, including fetal bovine serum (FBS), Roswell Park Memorial Institute (RPMI) 1640 medium, Dulbecco's modified Eagle medium (DMEM), DMEM/F12, penicillin, streptomycin, Phosphate-buffered saline (PBS), and trypsin, were obtained from Gibco Life Technologies. Phorbol 12-myristate 13-acetate (PMA) (HY-18739), 2-Mercaptoethanol (HY-Y0326) and FITC (HY-66019) were obtained from MedChemExpress. Human Fc Block antibody (Fc1.3216), BV421 Mouse Anti-Human CD68 (564 943), APC Mouse Anti-Human CD86 (555 660), and Fixation/Permeablization Kit (554 714) were purchased from BD Pharmingen. Gelatin (Type B, gel strength ≈300 g Bloom, from porcine skin) and glutaraldehyde (25 wt.% in H2O) were purchased from Sigma-Aldrich. Acetone, hydrochloric acid (HCl, 6 M), sodium carbonate (≥99.9%), sodium bicarbonate (≥99.9%), methacrylic anhydride (MA, 94%), sodium chloride (NaCl, ≥ 99.5%), sodium hydroxide (NaOH, ≥ 96%), 1-[3-(Dimethylamino) propyl]-3-ethylcarbodiimide Hydrochloride (EDC), N-hydroxy-succinimide (NHS), and phosphate buffer saline (PBS) were purchased from Titan Scientific. Guanidine hydrochloride (99%), potassium persulfate (KPS, 99%), styrene (99%), and 2-Methacryloyloxyethyl phosphorylcholine (MPC, 98%) were supplied by J&K Chemicals. Rabbit anti-human C3 antibody (BM4961), rabbit anti-human TNF-α antibody (BA0131), rabbit anti-human JNK1/2/3 antibody (BM4329), rabbit anti-human phospho-JNK1/2/3 antibody (T183+T183+T221) (BM4380), rabbit anti-human MMP-13 antibody (BA2204), and enzyme-linked immunosorbent assay (ELISA) kits of MMP-13 (EK0468), IL-1β (EK0392), IL-6 (EK0410), and TNF-α (EK0525) were provided by Boster Biological Technology. SDS-PAGE and western blot-related reagents were purchased from Epizyme Biotech. Rabbit anti-human CD11b antibody (48893S), rabbit anti-human CD86 antibody (91 882), rabbit anti-human p38 MAPK antibody (8690S), rabbit anti-human phospho-p38 MAPK antibody (4511S), rabbit anti-human p44/42 MAPK (ERK) antibody (4695S), rabbit anti-human phospho-p44/42 MAPK (p-ERK) antibody (4370S), rabbit anti-human GAPDH antibody (HRP conjugate) (8884S), and anti-rabbit IgG HRP-linked secondary antibody (7074S) were obtained from Cell Signaling Technology. Mouse anti-human CD68 anti-human antibody (66231-2-Ig) was obtained from Proteintech Group, Inc. Rabbit anti-human Col II antibody (ab34712) and Alexa Fluor 647-labeled anti-human C3 antibody (ab196639) were obtained from Abcam. Lipofectamine 3000, macrophage colony-stimulating factor (M-CSF) (PeproTech, 315-02), and qPCR-related reagents, such as TRIzol reagent, DEPC-treated water, TB Green Premix Ex Taq, and PrimeScript RT Master Mix, were purchased from Thermo Fisher Scientific.

Cell Culture: For BMDMs culture, dissected femurs were flushed out with PBS to collect bone marrow cells. Cells were then washed twice with PBS and cultured in in DMEM with 10% FBS, 1% penicillin-streptomycin (P/S), and 20 ng mL^{-1} M-CSF. Fresh medium with M-CSF was supplied on day 3 and day 5, and cells were ready for subsequent assays on day 7. THP-1 cells were cultured in RPMI 1640 medium with 10% FBS and 1% P/S. THP-1 cells were differentiated with 100 ng mL^{-1} PMA for 72 h prior to each experiment, and then the medium was exchanged with fresh medium without PMA. Cells were maintained in a cell culture incubator with 5% CO_2 at 37 °C. For C28/I2 cell culture in conditioned medium, NPs were first co-cultured with differentiated THP-1 cells for 4 h as described. Afterward, the NP-containing medium was replaced with fresh complete RPMI-1640 medium and cultured for an additional 48 h, allowing THP-1 cells to release soluble factors into the medium, which became the conditioned medium. Then, C28/I2 cells were seeded and cultured with the conditioned medium to assess the impact of THP-1 cell and NP-derived factors on C28/I2 cells. After 48 h of incubation with the conditioned medium, C28/I2 cells were washed with PBS and processed for immunofluorescence or qPCR to evaluate chondrogenic gene expression.

RNA-Seq for BMDMs: The total RNA of BMDMs (treated with or without 2 mg mL^{-1} PS-NPs for 48 h) was extracted using TRIzol reagent according to the manufacturer's instructions. KEGG pathway analysis, gene heatmap, and GO analysis were performed via standard transcriptome analysis.

Construction of Human Synovial Tissue Explants and Immunofluorescence: Human synovial membranes obtained at knee arthroplasty in OA patients were established as synovial explants. Prior to further processing, synovial membrane membranes were cut into pieces at equal volume and washed with sterile PBS three times and cultured in DMEM containing 1% P/S, 1% ITS, and 50 µg mL^{-1} L-proline. The explants respectively received opsonized PS-NPs at different concentration or Gel-NPs, PS-PMPC, and Gel-PMPC treatment for 48 h. Then, the explants were collected and washed with PBS for 3 times to remove the NPs. For immunofluorescence experiments, explants were washed with PBS and fixed in 4% paraformaldehyde overnight. Next, the fixed tissues were rinsed with PBS and immersed in 30% sucrose at 4 °C until they sink. Then, the tissues were embedded in optimal cutting temperature compound and were cut 20-µm thick sections using a cryostat at − 20 °C. Subsequently, the tissue sections received air-dry for 30 min at room temperature and were incubated the sections with blocking solution (5% normal goat serum and Triton X-100) for 1 h at room temperature to block nonspecific binding sites and permeabilize the cells. Then, the diluted primary antibodies for CD11b (1:200), CD68 (1:200), and CD86 (1:200) were applied to incubate the sections overnight at 4 °C in a humidified chamber. Diluted fluorescently labeled secondary antibodies (Alexa Fluor 555-conjugated donkey anti-rabbit for CD11b, 1:500, Alexa Fluor 488-conjugated goat anti-mouse for CD68, 1:500, and Alexa Fluor 555-conjugated donkey anti-rabbit for CD86 1:500) were used to incubate the sections for 2 h at room temperature. The nuclei were stained with 1 mg mL^{-1} DAPI for 10 min at room temperature. Finally, stained sections were observed under confocal microscope (Nikon AXR NSPARC) for CD11b, CD68, or CD86 using appropriate filters and settings. ImageJ software was used to calculate the fluorescence intensity of CD11b, CD68, or CD86.

Opsonization of NPs in Synovial Fluids: Human synovial fluids were collected from OA patient donors in knee arthroplasty by separation from clotted blood, and adhering to strict precautions to preserve the functional complement protein. PS-NPs at different mass (5, 10, 20 mg) or other NPs (Gel-NPs, PS-PMPC, Gel-PMPC, 10 mg) were added to the synovial fluids (1 mL) for incubation 37 °C for 30 min. Then the NPs were washed with PBS at 12 000 × g at 4 °C using centrifuge (Eppendorf) and resuspended in 1 mL DMEM for further cell co-culture. For the specific blockade of C3, synovial fluids were pretreated with an anti-C3 neutralizing antibody (5 µg mL^{-1}) or Compstatin (20 µM) at 37 °C for 2 h before NPs incubation.

Observation of Macrophage Phagocytosis for Opsonized NPs: Differentiated THP-1 cells were plated in 24-well microplate at a density of 10^5 cells per well, with the addition of 500 µL DMEM containing opsonized NPs. Plates were then transferred to a cell culture incubator, and the cells were collected 4 h later. The lysosomes in cells were stained with LysoTracker Red following the manufacturer's instructions. For CD11b detection, THP-1 cells were fixed with 4% paraformaldehyde and stained with rabbit anti-human CD11b overnight. Subsequently, the cells were incubated with Alexa Fluor 555 donkey anti-rabbit IgG (H+L) secondary antibody for 2 h and observed by confocal microscope (Nikon AXR NSPARC). Flow cytometry was used to quantitively evaluate the phagocytosis for NPs. Briefly, THP-1 cells were harvested and washed by PBS three times, and fixed in using Fixation/Permeabilization Kit. All cells were blocked with Human Fc Block antibody. The antibodies used for flow cytometry were BV421 Mouse Anti-Human CD68 and APC Mouse Anti-Human CD86. The stained pellets were resuspended in 200 µL of FACS buffer immediately prior to flow cytometry analysis (BD FACSVerse flow cytometer). Data were gated on FSC versus SSC and FSC (height) versus FSC (area) to exclude debris and doublets. FITC staining gelatin-based NPs fluorescence in THP-1 cells was quantified by mean fluorescence intensity.

Specific Blocking and Gene Silencing for CD11b: THP-1 cells were cultured and induced differentiation by PMA as described in Cell culture for 3 days. For Specific blocking, rabbit isotype IgG or CD11b antibody was added to the culture medium at a final concentration of 5 µg mL^{-1}. For CD11b silencing, the knockdown efficiency of three siRNA sequences was first assessed, and two of them were selected (sequences of siCD11b are shown in Table S1, Supporting Information). siRNA was mixed with Lipofectamine 3000 transfection reagent at a final concentration of 100 nM. After 48 h, the medium was exchanged with fresh medium containing opsonized NPs for observation of phagocytosis for NPs.

Detection of C3 Opsonization on NPs Surface: The opsonized C3 on NPs surface in human synovial fluids was measured by immuno-dot-blot or western blot assay according to previous report.[44] NPs in PBS were added into the synovial fluids at final concentration 10 mg mL^{-1}. EDTA was added to the synovial fluids before the addition of NPs. After incubation for 30 min at 37 °C, NPs were washed three times with PBS at 12 000 g at 4 °C using centrifuge (Eppendorf) and were resuspended in 20 μL^{-1} PBS. For direct observation, Alexa Fluor 647-labeled C3 antibody was added to the resuspended NPs (1:100) for incubation for 2 h. Then, NPs were washed and imaged with a confocal microscope (Nikon AXR NSPARC). For dot blot assay, 2 µL aliquots were applied onto a 0.45-µm-pore nitrocellulose membrane. For Western blot assay, NPs after washing were resuspended in reducing sample buffer, boiled for 10 min at 95 °C and separated on a 4–20% Tris-Glycine SDS-PAGE at 120 V for 60 min. The proteins were transferred to polyvinyl difluoride (PVDF) membrane at 400 mA for 30 min. For detection of C3, the membranes were blocked with a blocking buffer of 5% w/w nonfat dry milk in TBS-T (1x TBS and 0.1% v/v Tween-20) for 1 h at room temperature, probed with C3 antibody (1:1000) for 1 h at room temperature. The membranes were washed three times with TBS-T solution, and HRP-conjugated secondary antibodies were treated (1:10 000) for 1 h while shaking. The results were developed using Omni-ECL Light Chemiluminescence Kit in an imaging system (Amersham ImageQuant 800) and analyzed semi-quantitatively using ImageJ software.

Synthesis of PS-NPs and Gel-PMPC: PS-NPs were synthesized via conventional emulsion polymerization. First, KPS (initiator, 0.74 g) and SDS (surfactant, 0.48 g) were dissolved in 150 mL of deionized water. Then 10 g of styrene was added into the solution, and the polymerization was conducted under a nitrogen atmosphere for 2 h at 80 °C. Finally, PS-NPs was obtained by dialysis against deionized water and lyophilized. For synthesis of Gel-PMPC, 5 g of Gelatin was dissolved in 100 mL of deionized water at 40 °C, then 100 mL of acetone was added. The supernatant was discarded, and the precipitate was re-dissolved by 100 mL deionized water. Subsequently, the pH of the solution was adjusted to 2.5. Next, 300 mL of acetone was added dropwisely. The resulting colloidal particles were cross-linked by adding 505 of µL glutaraldehyde for 16 h. Then, 200 mL of guanidine hydrochloride solution (0.1 M) was added and stirred for 1h. The resulting Gel-NPs were washed with deionized water for three times by centrifugation (10 000 rpm for 1 h). Methacrylic anhydride (1.16 mL g of Gel-NPs) was then added to a 10 mg mL^{-1} Gel-NPs solution in 0.1 M carbonate bicarbonate buffer and stirred for 1 h at 50 °C. The resultant (named Gel-MA) was purified by dialysis against water for 3 days. Thereafter, 3 mg KPS was dissolved in 80 mL of 10 mg mL^{-1} Gel-MA solution, and 50 mg HMEM dissolved in 2.5 g acetone was added. The reaction was carried out in the dark for 2 h, and the product (named Gel-HMEM) was purified by dialysis for 3 days and lyophilized. Subsequently, 100 mg Gel-HMEM and 500 mg MPC were dissolved in 10 mL water, adjusted to pH 4, deoxygenated with nitrogen for 10 min, and photo-polymerized under UV–vis light (175 W) for 2 h. Finally, Gel-PMPC was obtained by dialysis and lyophilized.

Synthesis of FITC Labeled Gel-PMPC and PS-PMPC: For FITC-Gel-NPs, 5 g of gelatin and 10 mg of FITC were dissolved in 50 of mL Na_2CO_3 buffer, and the solution was stirred at 40 °C for 8 h in the dark. The FITC modified gelatin solution was obtained after dialysis against deionized water. The FITC-Gel-NPs were then prepared by the previously described method. For FITC-PS-NPs, 5 g of PS-NPs was dispersed in 50 mL of ethanol and sonicated for 30 min to ensure thorough dispersion. Subsequently, 5 mg of FITC was added to the mixture, and the suspension was stirred for 8 h in the dark. The final product was obtained after dialysis against deionized water.

Characterization of Gel-PMPC: The size and size distribution of the nanoparticles were measured on a NICOMP 380 ZLS instrument. The morphology was conducted with a field emission SEM (GeminiSEM 500, Germany) and a JEM-1400 TEM. Zeta potential was measured using a Zetasizer instrument (Malvern Instruments, ZEN 3700, UK) at room temperature; the sample was dispersed in a HEPES buffer solution (5 mM, pH = 7), and the Smoluchowski mathematical model was employed to calculate the zeta potential value. ^{1}H NMR spectra were recorded by a Bruker Ascend 600 MHz spectrometer (chemical shifts relative to TMS). Fourier transform infrared spectrometer (FTIR) spectra were recorded by a Nicolet iS20 FTIR using powder-pressed KBr pellets. Light scattering measurement was tested with an ALV light scattering apparatus, equipped with a 21 mW He-Ne laser operating at a wavelength of 632.8 nm. The chemical state of the elements was analyzed by an XPS spectrometer (Thermo Scientific K-Alpha) using an Al Kα X-ray source. The surface elements of the samples were conducted by an X-ray photoelectron spectroscopy (XPS, Thermo Scientific K-Alpha, USA). The collected data was calibrated by the standard C 1s peak at 284.8 eV.

Cartilage Preparation and Lubrication Test: The cartilage samples were prepared as reported protocol.[9] One group of cartilage samples was incubated in the lubricant solution at 4 °C for 1 day before the lubrication testing was performed. The porcine cartilage samples were subjected to treatment with 0.5% trypsin solution for 24 h to mimic OA. The lubrication properties of Gel-NPs and Gel-PMPC were characterized using rotational configuration to minimize ploughing and fluid pressure effects. Briefly, a plastic Petri dish (10 cm in diameter) was glued by cyanoacrylate to the bottom metal fixture surface. The 6.0 mm sample surface was fixed on top of the 9.0 mm surface. To ensure sufficiently contact between the sample surfaces, the upper sample was lowered and pressed against the bottom sample until a load value of ≈0.01 N was reached. The corresponding recorded height, which was automatically sensed by rheometer, was used to calculate the 18% compression height. The samples were then bathed in the lubricant solution to be tested and maintained the strain for 60 min. After 1 200 s of pre-sliding duration, the cartilage samples were allowed to rotate + 2 revolutions and then − 2 revolutions at a sliding viscosity of 0.3 mm s^{-1}. Torque (τ) and normal force (F) were measured during the test, and the friction coefficient was calculated by following equation: $\mu = \tau/RF$. The kinetic friction coefficient of the cartilage sample was derived from the average value over the course of the second rotation, and the static friction coefficient was also calculated from the maximum torque during the start-up period. While we acknowledge that rheometers may not fully replicate the physiological conditions in vivo, this method provides a reproducible and widely accepted approach for evaluating the lubrication performance of biomaterials under controlled contact conditions.[7a,23] Future studies employing specialized tribological platforms (e.g., reciprocating systems with controlled load and motion)[45] will be valuable for further validating the lubrication performance of Gel-PMPC.

In Vitro Macrophage Uptake of Gel-PMPC: For flow cytometry (BD Accuri C6), opsonized NPs in synovial fluids were co-cultured with THP-1 cells. After 4 h, the cells were collected and fixed in 4% paraformaldehyde for 15 min and resuspended in labeled antibody diluted in FACS buffer. To stain fixed cells, 100 µL aliquots of cell suspensions were pelleted 300 × g for 5 min, then resuspended in labeled antibody diluted in FACS buffer (1:500 dilution for APC-anti-CD68). Samples were incubated with staining antibodies for 20 min at room temperature in the dark, diluted with 1 mL of FACS buffer, and pelleted at 500 × g for 5 min. The stained pellets were resuspended in 200 µL of FACS buffer immediately prior to flow cytometry analysis (BD Accuri). Data were gated on FSC versus SSC and FSC (height) versus FSC (area) to exclude debris and doublets. FITC staining Gelatin-based NPs fluorescence in THP-1 cells was quantified by mean fluorescence intensity, gated on FITC-positive populations.

Macrophage Polarization, ROS Generation, Mitochondria Potential and Western Blot Analysis: After opsonized NPs were co-cultured with THP-1 cells for 4 h, the medium was exchanged with fresh total RPMI 1640 medium for another 48 h incubation.

For macrophage polarization analysis, cells were collected and received fixation, permeabilization, and blocking. Then, cells were incubated with the primary antibodies against CD68 (1:200) and CD86 (1:200) overnight at 4 °C. After washing three times with PBS, the samples were incubated with appropriate fluorescent secondary antibodies for 2 h. The nuclei were stained with 1 mg mL^{-1} DAPI for 10 min at room temperature. Finally, the cells were imaged by confocal microscope (Nikon AXR NSPARC). For assessment of ROS generation, cells after co-culture were washed three times with PBS. ROS Assay Kit was used according to the manufacturer's protocol. The level of ROS within cells was observed under a confocal microscope and was quantified by mean fluorescence intensity in FITC

channel through FCM. For evaluation of mitochondria potential, mitochondrial membrane potential assay kit with JC-1 was used according to the manufacturer's protocol. The cells were washed at least thrice before analyzing. Qualitative estimation of red and green fluorescence was evaluated by observing the treated and JC-1-stained cells under CLSM analyzed semi-quantitatively using ImageJ software. The red fluorescence represents the potential dependent JC-1 aggregation and green fluorescence represents the JC-1 monomers. The decreasing red/green fluorescence ratio indicates the mitochondrial membrane depolarization. For western blot assay, total protein from THP-1 cells was extracted using RIPA lysis buffer consisting of protease and phosphatase inhibitors. The protein concentrations were detected using a BCA protein assay kit. Equal amounts of protein (20 µg) were diluted in loading buffer. The membranes were incubated with ERK1/2, phosphor-ERK1/2 (p-ERK1/2), JNK1/2/3, p-JNK1/2/3, p38, p-p38 (diluted 1: 1000), and GAPDH (diluted 1: 2000) primary antibodies overnight at 4 °C. The other procedure of Western blot is described in the Detection of C3 opsonization on NPs surface.

ELISA: Synovial explants were collected and rinsed with pre-chilled PBS for 3 times and received weighing. Small volume of liquid nitrogen was added to the mortar and the tissue was ground, and the powdered tissue was transferred to homogenization buffer for incubation on ice (30 min), with occasional vortexing to ensure complete lysis of the tissue. Then, the lysate was centrifuged at 12 000 × *g* for 10 min at 4 °C to pellet debris and unbroken cells, and the supernatant was transferred. The concentrations of IL-1β, IL-6, and TNF-α were determined by ELISA according to the manufacturer's protocol. The associated protein concentration of each sample was calculated using the reference standard curve.

qPCR Analysis of Pro-Inflammatory Factors: The levels of chondrogenesis genes (Col II, SOX9, and aggrecan) were measured by qPCR assay. Cells were harvested and treated with Trizol for RNA extraction. PrimeScript RT Master Mix was used to generate cDNA. qPCR assay was performed with TB Green Premix Ex Taq. The relative gene expression was calculated, normalized to GAPDH, and compared using the $2^{-\Delta\Delta CT}$ method (sequences of the primers are shown in Table S2, Supporting Information).

Biocompatibility Evaluation of Gel-PMPC: The in vitro biocompatibility of Gel-PMPC was evaluated using C-28/I2 human chondrocyte cells. C-28/I2 cells were seeded in 96-well plates at a density of 1×10^4 cells per well and incubated overnight, and then were treated with varying concentrations of Gel-PMPC (0, 2, 5, and 10 mg mL^{-1}) for 48 h. Finally, Cell viability was assessed using the CCK-8 and live/dead staining assay following the manufacturer's instructions. For the in vivo biocompatibility evaluation of Gel-PMPC, Sprague-Dawley (SD) rats ($n = 3$ per group) were intra-articularly injected with Gel-PMPC (2, 5, or 10 mg mL^{-1}, 100 µL per joint), while control groups received saline injections. After 4 weeks, rats were euthanized, and major organs (heart, liver, spleen, lung, kidney) were harvested and fixed in 4% paraformaldehyde. Tissue sections were stained with H&E and examined for histopathological changes. Additionally, blood samples were collected via cardiac puncture for hematological and biochemical analysis. Blood cell counts and biochemical indicators of liver function and kidney function were analyzed using a biochemical analyzer.

Treatment Effects of Gel-PMPC in Rat Models of OA: SD male rats (12-weeks old) were obtained from SLAC Laboratory Animal CO. LTD. Animals were anesthetized using pentobarbital sodium at a dosage of 30 mg $k^{-1}g$. Following appropriate skin preparation, the knee joint was exposed via a medial parapatellar incision, and the joint capsule was opened. The anterior cruciate ligament was transected using micro-scissors. The animals were then randomly divided into four groups ($n = 6$ per group): a PBS-treated group; a Gel-NPs-treated group; a PS-PMPC-treated group; and a Gel-PMPC-treated group. Four weeks after surgery to establish osteoarthritis, 100 µL of sterile saline, 10 mg mL^{-1} Gel-NPs solution, 10 mg mL^{-1} PS-PMPC solution, or 10 mg mL^{-1} Gel-PMPC solution was injected into the postoperative joints biweekly, starting on day 0. For comparison, normal healthy rat knees that did not receive either surgery or intra-articular injections served as the sham-operated control group. The in vivo retention of the NPs was tested in ALCT-operated rats. The rats ($n = 3$ per group) were injected with 100 µL of Cy5-labeled Gel-NPs-PS-PMPC or Gel-PMPC (10 mg mL^{-1}) in the OA hind limb, while saline was used as a control solution. At designated time points, rats were imaged with an IVIS Lumina III imaging system. Fluorescence intensities were analyzed with Living Image software and normalized to the initial fluorescence signal after NPs injection.

Gait Analysis: Catwalk system (Shanghai, China) was used to analyze detailed gait parameters according to the manufacturer's protocol at 8 weeks post-operation. The gait of all rats who successfully ran uninterrupted was recorded and analyzed using Catwalk software. The illustration of the motion path, footprint pressure heat map, run duration, and run average speed was evaluated for all four limbs. The pawprint length, width, and area were assessed for all right posterior legs.

Micro-CT Analysis: All collected joint tissues were collected and fixed with 4% paraformaldehyde. For micro-CT analysis, all samples were scanned and reconstructed using an imaging system (microCT Quantum GX2, Revvity). 3D images of the tibial subchondral bone were reconstructed using CTvox software (USA). The volume of osteopyte and BV/TV (%) were acquired using DataViewer and CTAn software (USA).

Histological, Immunohistochemical, and Immunofluorescence Stainings: After being decalcified with EDTA for 4 weeks, the samples dehydrated in ethanol were embedded in paraffin and sliced into 5-µm sections. The SO&FG staining was performed to evaluate the articular cartilage degeneration. The Osteoarthritis Research Society International-modified Mankin criteria, as previously reported,[46] were calculated by three authors who were blinded to all sample information, to grade articular cartilage degeneration. Immunohistochemical staining was performed using the anti-Col2 and anti-MMP-13 antibody to evaluate the expression of Col II and MMP-13 in the articular cartilages and anti-TNF-α antibody to evaluate the expression of TNF-α in the synovial membranes. The following formula was used to calculate the optical density score (ODS) for the immunohistochemistry images. ODS = (high positive (%) × 4 + positive (%) × 3 + low positive (%) × 2 + negative (%) × 1) /100. Immunofluorescence staining was demonstrated using the anti-CD68 and anti-CD86 antibodies to evaluate the expression of CD68 and CD86 in the synovial membranes. The related relative Col II, MMP-13, TNF-α, and ratio of CD86/CD68 were obtained by the ImageJ software.

Statistical Analysis: All experiments were repeated 3 times with data reported as the mean ± s.d. Statistical analysis was performed using Graphpad Prism. When analyzing the data, it was first tested whether the data of each group conformed to normal distribution and homogeneity of variance. After confirming that all the data in each group were in line with normal distribution and homogeneity of variance, the one-way analysis of ANOVA was carried out for the groups receiving different treatments, while unpaired Student's *t* test was employed within two groups. Statistical significance was considered significant for $*p < 0.05$, $**p < 0.01$, $***p < 0.001$, and $****p < 0.0001$.

Ethical Statement

The collection of human osteoarthritic cartilages and synovium tissues samples was approved by the Ethics Committee of Zhongshan Hospital of Fudan University (clinical donation, No. Y2024-1088). The animal experiments received approval from the institutional Animal Care and Use Committee at Zhongshan Hospital, Fudan University.

Supporting Information

Supporting Information is available from the Wiley Online Library or from the author.

Acknowledgements

C.C., M.W., and L.W. contributed equally to this work. This work was supported by the National Key Research and Development Program of

China (2024YFC3044700), the National Natural Science Foundation of China (No. 82172413 and 82372393), "Science and Technology Innovation Action Program" of Shanghai Science and Technology Commission (23ZR1480300), Shanghai Hospital Development Center Foundation (No. SHDC12023111), Shanghai Pujiang Programme (23PJD024), the National Natural Science Foundation of China for Young Scholars (21706074), National Key Research and Development Program of China (2023YFD1700303), the Science and Technology Innovation Program of Hunan Province (2024RC7001), State Key Laboratory of Chemical Engineering (No. SKL-ChE-24C01).

Conflict of Interest

The authors declare no conflict of interest.

Author Contributions

C.C., M.W., and L.W. performed most of the experiments, discussed the results, and wrote the manuscript. J.G. provided technical support for lubrication test. L.W., Y.Z, G.W., B.H., and L.C. assisted in the establishment of animal model and analyzed tools. M.S, M.W., X.G., L.C., and Z.Y. helped in conceiving the project, designing the experiments, and supervising the participants of this study. S.L, L.C., and Z.Y. analyzed and interpreted the data.

Data Availability Statement

The data that support the findings of this study are available from the corresponding author upon reasonable request.

Keywords

complement C3, interface, macrophages, osteoarthritis, phagocytosis

Received: January 16, 2025
Revised: April 10, 2025
Published online:

[1] a) P. R. Coryell, B. O. Diekman, R. F. Loeser, *Nat. Rev. Rheumatol.* **2021**, *17*, 47; b) R. Barnett, *Lancet* **2018**, *391*, 1985.
[2] D. J. Hunter, S. Bierma-Zeinstra, *Lancet* **2019**, *393*, 1745.
[3] a) J. N. Katz, K. R. Arant, R. F. Loeser, *JAMA* **2021**, *325*, 568; b) D. J. Hunter, D. Schofield, E. Callander, *Nat. Rev. Rheumatol.* **2014**, *10*, 437.
[4] P. G. Conaghan, A. D. Cook, J. A. Hamilton, P. P. Tak, *Nat. Rev. Rheumatol.* **2019**, *15*, 355.
[5] a) Y. Yan, A. Lu, Y. Dou, Z. Zhang, X. Y. Wang, L. Zhai, L. Y. Ai, M. Z. Du, L. X. Jiang, Y. J. Zhu, Y. J. Shi, X. Y. Liu, D. Jiang, J. C. Wang, *Adv. Sci.* **2023**, *10*, 2207490; b) M. Rong, D. Liu, X. Xu, A. Li, Y. Bai, G. Yang, K. Liu, Z. Zhang, L. Wang, K. Wang, L. Lu, Y. Jiang, J. Liu, X. Zhang, *Adv. Mater.* **2024**, *36*, 2405641.
[6] a) W. Lin, J. Klein, *Adv. Mater.* **2021**, *33*, 2005513; b) X. He, S. He, G. Xiang, L. Deng, H. Zhang, Y. Wang, J. Li, H. Lu, *Adv. Mater.* **2024**, *36*, 2405943.
[7] a) R. Xie, H. Yao, A. S. Mao, Y. Zhu, D. Qi, Y. Jia, M. Gao, Y. Chen, L. Wang, D. A. Wang, K. Wang, S. Liu, L. Ren, C. Mao, *Nat. Biomed. Eng.* **2021**, *5*, 1189; b) C. Xie, Q. Sun, Y. Dong, H. Lu, W. Li, Z. Lin, K. Li, J. Cheng, Z. Liu, J. Qi, B. Tang, L. Lin, *ACS Nano* **2023**, *17*, 12842.
[8] a) M. J. Mitchell, M. M. Billingsley, R. M. Haley, M. E. Wechsler, N. A. Peppas, R. Langer, *Nat. Rev. Drug Discovery* **2021**, *20*, 101; b) S. Gordon, *Immunity* **2016**, *44*, 463.
[9] J. Yang, S. Li, Z. Li, L. Yao, M. Liu, K. L. Tong, Q. Xu, B. Yu, R. Peng, T. Gui, W. Tang, Y. Xu, J. Chen, J. He, K. Zhao, X. Wang, X. Wang, Z. Zha, H. T. Zhang, *Adv. Sci.* **2024**, *11*, 2304617.
[10] L. Wang, S. Quine, A. N. Frickenstein, M. Lee, W. Yang, V. M. Sheth, M. D. Bourlon, Y. He, S. Lyu, L. Garcia-Contreras, Y. D. Zhao, S. Wilhelm, *Adv. Funct. Mater.* **2024**, *34*, 2308446.
[11] a) E. Blanco, H. Shen, M. Ferrari, *Nat. Biotechnol.* **2015**, *33*, 941; b) S. Tenzer, D. Docter, J. Kuharev, A. Musyanovych, V. Fetz, R. Hecht, F. Schlenk, D. Fischer, K. Kiouptsi, C. Reinhardt, K. Landfester, H. Schild, M. Maskos, S. K. Knauer, R. H. Stauber, *Nat. Nanotechnol.* **2013**, *8*, 772.
[12] M. Mahmoudi, M. P. Landry, A. Moore, R. Coreas, *Nat. Rev. Mater.* **2023**, *8*, 422.
[13] A. Aderem, D. M. Underhill, *Annu. Rev. Immunol.* **1999**, *17*, 593.
[14] M. Y. Adler, I. Issoual, M. Rückert, L. Deloch, C. Meier, T. Tschernig, C. Alexiou, F. Pfister, A. F. Ramsperger, C. Laforsch, U. S. Gaipl, K. Jüngert, F. Paulsen, *J. Hazard. Mater.* **2024**, *471*, 134253.
[15] X. Liu, H. Zhang, B. Yan, K. W. K. Yeung, Y. Liao, L. Ouyang, X. Liu, *Adv. Sci.* **2023**, *10*, 2205048.
[16] Y. Li, S. Jacques, H. Gaikwad, G. Wang, N. K. Banda, V. M. Holers, R. I. Scheinman, S. Tomlinson, S. M. Moghimi, D. Simberg, *Nat. Nanotechnol.* **2024**, *19*, 246.
[17] Y. Li, G. Wang, L. Griffin, N. K. Banda, L. M. Saba, E. V. Groman, R. Scheinman, S. M. Moghimi, D. Simberg, *J. Controlled Release* **2021**, *338*, 548.
[18] C. D. Walkey, J. B. Olsen, H. Guo, A. Emili, W. C. Chan, *J. Am. Chem. Soc.* **2012**, *134*, 2139.
[19] C. M. Hu, R. H. Fang, K. C. Wang, B. T. Luk, S. Thamphiwatana, D. Dehaini, P. Nguyen, P. Angsantikul, C. H. Wen, A. V. Kroll, C. Carpenter, M. Ramesh, V. Qu, S. H. Patel, J. Zhu, W. Shi, F. M. Hofman, T. C. Chen, W. Gao, K. Zhang, S. Chien, L. Zhang, *Nature* **2015**, *526*, 118.
[20] Z. Wang, E. D. Hood, J. Nong, J. Ding, O. A. Marcos-Contreras, P. M. Glassman, K. M. Rubey, M. Zaleski, C. L. Espy, D. Gullipali, T. Miwa, V. R. Muzykantov, W. C. Song, J. W. Myerson, J. S. Brenner, *Adv. Mater.* **2022**, *34*, 2107070.
[21] a) H. Zhou, Z. Fan, P. Y. Li, J. Deng, D. C. Arhontoulis, C. Y. Li, W. B. Bowne, H. Cheng, *ACS Nano* **2018**, *12*, 10130; b) S. Peng, B. Ouyang, Y. Men, Y. Du, Y. Cao, R. Xie, Z. Pang, S. Shen, W. Yang, *Biomaterials* **2020**, *231*, 119680.
[22] M. Chen, W. H. Briscoe, S. P. Armes, J. Klein, *Science* **2009**, *323*, 1698.
[23] A. Singh, M. Corvelli, S. A. Unterman, K. A. Wepasnick, P. McDonnell, J. H. Elisseeff, *Nat. Mater.* **2014**, *13*, 988.
[24] H. Yang, R. Yan, Q. Chen, Y. Wang, X. Zhong, S. Liu, R. Xie, L. Ren, *J. Colloid Interface Sci.* **2023**, *652*, 2167.
[25] a) Y. Hui, X. Yi, D. Wibowo, G. Yang, A. P. J. Middelberg, H. Gao, C. X. Zhao, *Sci. Adv.* **2020**, *6*, aaz4316; b) P. Desai, R. Rimal, A. Florea, R. A. Gumerov, M. Santi, A. S. Sorokina, S. E. M. Sahnoun, T. Fischer, F. M. Mottaghy, A. Morgenroth, A. Mourran PotemkinII, M. Möller, S. Singh, *Angew. Chem.* **2022**, *61*, 202116653.
[26] U. T. Do, J. Kim, Q. S. Luu, Q. T. Nguyen, T. Jang, Y. Park, H. Shin, N. Whiting, D. K. Kang, J. S. Kwon, Y. Lee, *Carbohydr. Polym.* **2023**, *304*, 120490.
[27] F. Chen, G. Wang, J. I. Griffin, B. Brenneman, N. K. Banda, V. M. Holers, D. S. Backos, L. Wu, S. M. Moghimi, D. Simberg, *Nat. Nanotechnol.* **2017**, *12*, 387.
[28] a) Y. Sun, Y. Han, Y. Dou, X. Gong, H. Wang, X. Yu, Q. Wang, Y. Wang, Y. Dai, F. Ye, W. Jin, H. Zhang, *Bioact. Mater.* **2022**, *14*, 120; b) X. Zhang, W. Chen, X. Zhu, Y. Lu, *ACS Appl. Mater. Interfaces* **2017**, *9*, 7972.
[29] a) D. Acharya, X. R. L. Li, R. E. Heineman, R. E. Harrison, *Front Immunol* **2020**, *10*, 3049; b) G. Hajishengallis, J. D. Lambris, *Immunol. Rev.* **2016**, *274*, 233.

[30] H. Zhang, C. Lin, C. Zeng, Z. Wang, H. Wang, J. Lu, X. Liu, Y. Shao, C. Zhao, J. Pan, S. Xu, Y. Zhang, D. Xie, D. Cai, X. Bai, *Ann. Rheum. Dis.* **2018**, *77*, 1524.
[31] U. C. Anozie, P. Dalhaimer, *Adv. Drug Delivery Rev.* **2017**, *122*, 65.
[32] H. Li, Y. Yuan, L. Zhang, C. Xu, H. Xu, Z. Chen, *Adv. Sci.* **2024**, *11*, 2305363.
[33] X. Zhang, L. Fan, J. Wu, H. Xu, W. Y. Leung, K. Fu, J. Wu, K. Liu, K. Man, X. Yang, J. Han, J. Ren, J. Yu, *J. Hepatol.* **2019**, *71*, 163.
[34] Y. Liu, R. Hao, J. Lv, J. Yuan, X. Wang, C. Xu, D. Ma, Z. Duan, B. Zhang, L. Dai, Y. Cheng, W. Lu, X. Zhang, *Bone Res.* **2024**, *12*, 15.
[35] C. R. Scanzello, S. R. Goldring, *Bone* **2012**, *51*, 249.
[36] W. Tong, Y. Zeng, D. H. K. Chow, W. Yeung, J. Xu, Y. Deng, S. Chen, H. Zhao, X. Zhang, K. K. Ho, L. Qin, K. K. Mak, *Ann. Rheum. Dis.* **2019**, *78*, 551.
[37] D. Nemirov, Y. Nakagawa, Z. Sun, A. Lebaschi, S. Wada, C. Carballo, X. H. Deng, D. Putnam, L. J. Bonassar, S. A. Rodeo, *Am. J. Sports Med.* **2020**, *48*, 624.
[38] C. D. DeMoya, A. Joenathan, T. B. Lawson, D. T. Felson, T. P. Schaer, M. Bais, M. B. Albro, J. Mäkelä, B. D. Snyder, M. W. Grinstaff, *Nat. Rev. Rheumatol.* **2024**, *20*, 432.
[39] Y. Lei, X. Wang, J. Liao, J. Shen, Y. Li, Z. Cai, N. Hu, X. Luo, W. Cui, W. Huang, *Bioact. Mater.* **2022**, *16*, 472.
[40] C. J. O'Conor, H. A. Leddy, H. C. Benefield, W. B. Liedtke, F. Guilak, *Proc. Natl. Acad. Sci. U. S. A.* **2014**, *111*, 1316.
[41] A. J. Rao, E. Gibon, T. Ma, Z. Yao, R. L. Smith, S. B. Goodman, *Acta Biomater.* **2012**, *8*, 2815.
[42] N. Gerwin, A. M. Bendele, S. Glasson, C. S. Carlson, *Osteoarthritis Cartilage* **2010**, *18*, S24.
[43] I. A. Jones, R. Togashi, M. L. Wilson, N. Heckmann, C. T. Vangsness Jr., *Nat. Rev. Rheumatol.* **2019**, *15*, 77.
[44] V. P. Vu, G. B. Gifford, F. Chen, H. Benasutti, G. Wang, E. V. Groman, R. Scheinman, L. Saba, S. M. Moghimi, D. Simberg, *Nat. Nanotechnol.* **2019**, *14*, 260.
[45] a) L. Xiang, J. Liang, Z. Wang, F. Lin, Y. Zhuang, Q. Saiding, F. Wang, L. Deng, W. Cui, *Sci. Adv.* **2023**, *9*, adc9375; b) H. Chen, T. Sun, Y. Yan, X. Ji, Y. Sun, X. Zhao, J. Qi, W. Cui, L. Deng, H. Zhang, *Biomaterials* **2020**, *242*, 119931; c) Y. Yao, G. Wei, L. Deng, W. Cui, *Adv. Sci.* **2023**, *10*, 2207438.
[46] Z. Cui, J. Crane, H. Xie, X. Jin, G. Zhen, C. Li, L. Xie, L. Wang, Q. Bian, T. Qiu, M. Wan, M. Xie, S. Ding, B. Yu, X. Cao, *Ann. Rheum. Dis.* **2016**, *75*, 1714.